NIST-GCR-93-628

Study of Fire Induced Flow Along the Vertical Corner Wall. Part 2

Kozo Saito

Grant 60NANB1D1142

NIST

NIST-GCR-93-628

Study of Fire Induced Flow Along the Vertical Corner Wall. Part 2

Kozo Saito

University of Kentucky
Department of Mechanical Engineering
Lexington, KY 40506-0108

Final Report
April 1993

Sponsored by:
U.S. DEPARTMENT OF COMMERCE
Technology Administration
National Institute of Standards
and Technology
Building and Fire Research Laboratory
Gaithersburg, MD 20899

U.S. DEPARTMENT OF COMMERCE
Ronald H. Brown, Secretary

NATIONAL INSTITUTE OF STANDARDS AND TECHNOLOGY
Raymond G. Kammer, Acting Director

Notice

This report was prepared for the Building and Fire Research Laboratory of the National Institute of Standards and Technology under grant number 60NANB1D1142. The statements and conclusions contained in this report are those of the authors and do not necessarily reflect the views of the National Institute of Standards and Technology or the Building and Fire Research Laboratory.

FINAL REPORT: A STUDY OF FIRE INDUCED FLOW ALONG THE VERTICAL CORNER WALL (PART II)
GRANT #60NANB1D1142

DR. HENRY MITLER, TECHNICAL OFFICER
BUILDING AND FIRE RESEARCH LABORATORY
NATIONAL INSTITUTE OF STANDARDS AND TECHNOLOGY
GAITHERSBURG, MD 20899

by

Kozo Saito, Associate Professor
Tel: (606)257–1685; FAX: (606)258–1035

Contents

Automated Infrared Imaging Temperature Measurement (pages 1–12 with twelve figures)

Fire–Induced Flow along the Vertical Corner Wall (pages 13–18)

Appendix – A: Measurements of Temperature Distribution and Heat Flux at a Vertical Corner wall surface (twenty–five figures)

Appendix – B: Flame Height Measurement (two figures)

AUTOMATED INFRARED IMAGING TEMPERATURE MEASUREMENT

A. Arakawa, K. Saito and W.A. Gruver

Combustion and Fire Research Laboratory
Department of Mechanical Engineering
and Center for Robotics and Manufacturing Systems
University of Kentucky
Lexington, KY 40506

ABSTRACT

This paper describes a new experimental technique with wide application which has been proven for corner fires. To measure the flame spread rate of pyrolysis front along vertically oriented flat and corner walls, it may be necessary to measure transient temperature profiles on the walls. Conventional thermocouple and visual observation methods, however, have limitations due to complexity of implementation and the inherent ambiguity of visual observations due to interference from flames. To overcome these limitations, automated infrared imaging was applied for simultaneously collecting temperature data in a relatively large wall surface area. Results indicate that the infrared system with a ($10.6 \pm 0.5\mu$m) band–pass filter successfully avoids the flame interference allowing measurements of temperature distribution on the fire–heated wall, from which the spread rate in any direction can be deduced. The infrared camera without filters also can be used to measure visible flame position as photographic and video camera.

INTRODUCTION

Upward flame spread is a severe phenomenon due to its rapid growth rate and radiant emission from the flame [1–8]. Past studies, both experimental and theoretical, were focused on upward flame spread over vertical flat walls, where two dimensional flame behavior is usually observed and a one dimensional spread rate model is applicable with reasonable accuracy [2,3,5].

The modeling of upward flame spread along a vertical corner wall, however, requires additional considerations due to the transient three dimensional nature of the flow pattern which causes complex convective and radiative heat transfer to the wall [9–10]. This latter result suggests that a one dimensional flame spread model is no longer valid for corner wall fires.

To predict flame spread rate on vertical corner walls, the detailed temperature profile of the wall surface must be understood. Experiments [10] showed that the nature of the upward spread along a vertical corner wall is two dimensional, highly transient and unstable. Conventional thermocouple techniques, if applied, have limitations due to their complexity of implementation, and the uncertainty of pyrolysis temperature (particularly for charring materials), as can be seen in previous work [3,4]. Visual observation techniques which were previously applied for spread rate measurement [1,3,4] can produce ambiguous results in the determination of the transient pyrolysis front location.

To overcome the limitations associated with these conventional methods, infrared radiometry, which is useful for non–contact temperature measurement [11,12], was applied with automated image analysis to obtain transient temperature distributions. The infrared camera is located away from the fire source and it must measure temperature of the wall through the flame. The main difficulty faced is that the wall temperature is considerably lower than the flame temperature, and therefore the flame radiation causes interference (i.e., the infrared system would detect some intermediate

flame temperature instead of the wall). Previous application of infrared imaging was hampered by this difficulty.

To obtain a measurement of the wall surface temperature by minimizing the flame interference, four different band–pass filters (5, 6, 8, and 10.6 μm with a band pass width of $\pm$ 0.5 μm) were applied. Wall fire experiments were performed using a one–half scale room corner model designed in our laboratory [10,13] for the study of fire–induced flow. To generate relatively stable and controlled temperature condition, Marinite (non–combustible) corner walls were heated by either methane, propane or hexane flames which provide a constant (in time) heat flux to the wall. The infrared image obtained through the 10.6μm band–pass filter showed good agreement both with the thermocouple data and the infrared image data obtained without flame interference. Based on this, the infrared technique was applied to the measurement of upward flame spread.

To understand the limitations and accuracy of our infrared system, it was applied to different flame and wall material conditions; and the effects of flame temperature and flame emissivity on the results are discussed.

EXPERIMENTAL METHODS

Infrared Radiometry

A one–half scale corner wall model (1m in length x 1m in width x 1.6m in height) with Marinite walls was used for this experiment. A gas burner whose exit surface is 15cm x 15cm and height 5 cm was placed on the floor near the corner wall. A diagram of the apparatus is shown in Fig. 1 (for the details, see [10,13]). The infrared camera was located away from the fire source to acquire the $Wall_1$ temperature with passing through the flame and the $Wall_2$ temperature without passing through the flame. This can be done by placing the infrared camera close to the $Wall_2$ and away from the $Wall_1$ providing a large ϕ as shown in Fig. 1. Through the infrared camera under this setting,

two different infrared images can be obtained simultaneously, a nearly normal two–dimensional image on the $Wall_1$ and a nearly tangential image on the $Wall_2$. Then both images were transformed into two separate two–dimensional (with ϕ and $\theta = 90^0$) images.

A typical fire–heated wall temperature (< 600K) is considerably lower than the average flame temperature (1100K – 1200K) determined from the measured (axial and radial) temperature profiles for sooty laminar hydrocarbon–air diffusion flames [14,15]. At $Wall_1$ the infrared camera detects the flame temperature instead of the wall temperature. The flame effect consists of band emissions from excited gas molecules and continuous emission from soot particles. The band emissions are mostly from CO_2 and H_2O, and both have a "window" between 10 and 11μm where they have negligible emissions. If a band–pass filter whose band–pass width covers the above wave length range were applied with the infrared camera, the effects due to CO_2 and H_2O will be eliminated.

To minimize the flame interference effect due to soot radiation, the effects of flame temperature and optical thickness on the emissivity of flame were investigated. Exploratory tests on the corner wall fires and the videotaped flame structure data for vertically oriented flat wall fires [3,4] proved that the visible yellow flame thickness is no more than 5cm over the entire flame length. In addition, the soot particles only exist in the thin layer of the high temperature region [14,15], and they are not uniformly distributed across the flame thickness normal to the wall surface. Therefore, an effective optical thickness will be smaller than the visible flame thickness. Assuming the optical depth (L) as the flame thickness (5 cm) and one–half of the flame thickness (2.5 cm), the flame emissivity (ϵ) was estimated using Beer's law, $\epsilon = 1 - \exp(-k\beta L)$. Using this approach, an average flame emissivity, $\epsilon = 0.04$ for L = 5 cm and $\epsilon = 0.02$ for L = 2.5 cm were obtained, where $k\beta = 0.8m^{-1}$ based on an assumption that the radiative properties

of wall fires are equal to those of hexane pool fires [16].

Next, calculations were made to estimate the relative importance of the effect of radiation from the soot particles to that from the fire–heated walls, which will be the pyrolyzing walls if the materials are combustible. Employing a pyrolysis temperature of 600K, for flammable wall materials, plot was made [radiation from the wall]/[radiation from the soot particles] as a function of flame emissivity for the average flame temperatures 1100K and 1200K (Fig. 2). Figure 2 also contains the effect of four different band–pass filters on the above radiation fraction. These results indicate that if the flame emissivity, $\epsilon \leq 0.03$ (for 1100K) and $\epsilon \leq 0.02$ (for 1200K), the radiation from the soot particles will become approximately one order of magnitude less than that from the wall. Furthermore, optical depth dependence on wave length leads to low emissivity at long wave length [17].

As a result, this indicates that the use of infrared imaging system may be possible for mapping the transient wall temperatures induced by fires.

To experimentally check the above arguments, the infrared camera was located to facilitate comparison of temperature profiles on $Wall_1$ measured through the flame to those on $Wall_2$ measured without passing through the flame. Four different wave length filters (5, 6, 8 and 10.6 μm with band pass width $\pm$ 0.5μm) were employed to eliminate the effect of the flame; then the results were compared with those from $Wall_2$ and the wall temperature just after the burner flame was extinguished by a quick cut–off of fuel supply. To investigate the effects of band emissions and soot particles, tests were conducted using methane–air premixed (blue), propane–air premixed (blue), methane–air diffusion (yellow), propane–air diffusion (yellow) flames, and a 10cm diameter hexane pool flame (sooty–yellow). The five different wall materials tested were black painted Marinite (non–combustible), white color board (combustible), black card–board (combustible), transparent PMMA (combustible), and black painted PMMA

(combustible).

The orientation of the infrared camera in terms of azimuthal angle, ϕ, and zenith angl, θ, was calculated using the image of two reference points. The image was recorded on video tape, and then digitized. The digitized image was analyzed to obtain the exact temperature distribution on the wall.

Image Processing and Transformation

The video signal was digitized into 8–bit gray levels and stored for subsequent analysis. First, a smoothing operation was performed to remove noise in the image. Next, distorted temperature profile images due to inclined projection were corrected to $\phi = \theta = 90^{0}$ using transformation of coordinates. Finally, contour tracing was performed to obtain isothermal lines and deduce 3 dimensional perspective projections. The encoding and disk storage time for a 200 x 170 image is 2 seconds. This simple compression scheme greatly enhances the system capability to process a long sequence of images.

A coordinate system (x, y, z) is chosen and the origin O_1 of the screen coordinate system (ξ, η, ζ) is assumed to be fixed on the screen of the infrared camera [18]. Suppose that ${}^{S}Q(Q_{\xi}, 0, Q_{\zeta})$ on the screen is a projected point of $P(P_x, P_y, P_z)$ on the wall. It can be obtained that: $k(P - C) = R_s({}^{S}Q - f{}^{S}j)$, where, $k = Q - C / P - C$. Using these relationships, the positions on the wall corresponding to any points of the image can be calculated. The values of ϕ and θ can be calculated by specifying two points ${}^{S}Q_1$ and ${}^{S}Q_2$ corresponding to two known points P_1 and P_2 (for details, see [19]).

MEASUREMENT OF WALL TEMPERATURE WITH FLAME INTERFERENCE

The infrared camera was calibrated by focusing on a Marinite wall, which was painted in non–luster black and heated to temperatures up to 500K; during the heating surface temperature of the Marinite wall was monitored by a 100μm diameter

chromel–alumel thermocouple which was embeded just underneath the Marinite surface. In addition, a temperature controlled furnace (emissivity is approximately 1.0) is also used to calibrate the infrared camera at temperature up to 1400K. To systematically study the flame effect, five different flames (as explained earlier) from a blue methane–air premixed flame to a sooty hexane pool flame were used. Then, in order to remove the effects of the energy emitted by the flame, four narrow band–pass filters (5, 6, 8 and 10.6μm with a band–pass width $\pm$ 0.5μm) were installed in the infrared camera and the wall temperature profiles at $Wall_1$ and $Wall_2$ were simultaneously measured.

Figure 3 shows the temperature profiles of $Wall_1$ measured through the yellow methane–air diffusion flame (left–hand side) and $Wall_2$ measured without passing through the flame (right–hand side). These results reveal that temperature profiles using the 5, 6 and 8μm band–pass filters were largely distorted by the flame effect. But that obtained with the 10.6μm band–pass filter showed hardly any effects from the flame, resulting in good agreement with temperature profiles on $Wall_2$. Both temperature profiles should agree if the two walls were symmetrically heated by the flame and the filters could successfully remove the effect of the flame. The profiles of $Wall_1$ (Fig. 3a, and c–e), however, were disturbed by the flame; the wall temperature behind the flame was not monitored.

To further demonstrate the filter effects, four different infrared color images are shown in Fig. 4. The top two infrared images were obtained using a blue methane–air premixed flame; and the bottom two infrared images were obtained using a sooty hexane pool flame. The burner heat release rate 18 kW was used for methane flame; and approximate flame height for the hexane pool flame was 40 cm. Conditions (a) and (c) were obtained after the wall temperature achieved steady state condition. Condition (b) was obtained in 1s after the burner was turned off, and (d) was obtained in 4s after the pool flame was quenched. The infrared images (a) – (b) and (c) – (d) are in good

agreement, demonstrating that the infrared imaging system can measure the wall temperature through the flame, and without the flame interference.

To calculate the spread rate from the infrared images, the transient wall temperature was measured without passing through the flame. Figure 5 shows representative results of the transient wall temperature profiles measured every 20 seconds after the propane–air gas burner with a burner heat flux, 18 kW, was ignited. A progress rate of 100^{o}C isotherm for horizontal (X) and vertical (Z) directions was deduced and shown in Fig. 5b.

The result from Fig. 5 demonstrates for the corner wall fires that, if the time history of the wall temperature is measured by infrared imaging, then the flame spread rate in any direction can be deduced. To further demonstrate this, we designed cardboard corner walls, one wall surface is white and the other is black and both have the same dimensions (1.2 m long x 0.2 m wide x 0.002 m thick). The corner walls were ignited at the bottom and a time series of the wall temperature distributions were obtained using the infrared camera with the 10.6μm band–pass filter. The spread rate was almost the same between the white and black cardboard; and the temperature distributions on the cardboard surface were successfully obtained for both cases. Four images obtained at 20 second intervals are shown at the top in Fig. 6. A high speed video camera was simultaneously employed to record flame spread behavior to investigate an alternative use for spread rate measurement. The video images resulted in a complex time series of flame behavior, from which no accurate spread rate can be measured (video images obtained at corresponding time periods to the infrared images are shown at the bottom in Fig. 6).

SUMMARY AND CONCLUSIONS

(1) Infrared image analysis is an effective tool for studying phenomena associated with building fires. This study provides background information and experimental data to

support the use of the infrared camera system for instantaneous measurement of two dimensional transient wall temperatures.

(2) Both fire–heated wall (non spread) experiments and fire spread experiments indicate that the infrared image system is very useful for measurement of the pyrolysis–front spread rate in any direction and for any materials.

(3) To check the effect of emissivity of the materials on the infrared temperature, upward flame spread experiments were conducted using white color board, black color board, transparent PMMA, and black painted PMMA. These experiments showed that a constant emissivity (ϵ is nearly 1) can be used to determine the pyrolysis front temperature.

(4) However, prior to apply the infrared imaging system to many fire experiments which involves many different materials, further studies are needed to understand the effect of emissivity change during pyrolysis and combustion on the infrared temperature.

ACKNOWLEDGEMENTS

We wish to acknowledge M. Daikoku and A. Ito for their assistance in performing flame spread experiments and K. Lin for his assistance in developing image analysis system. This study was supported by the Building and Fire Research Laboratory, National Institute of Standards and Technology through Grant No. 60NANB0D1031.

REFERENCES

[1] Orloff, L., deRis, J. and Markstein, G.H., Fifteenth Symposium (Intl.) on Combustion, The Combustion Institute, 1975, pp. 183–192.

[2] Mitler, H., Twenty–third Symposium (Intl.) on Combustion, The Combustion Institute, 1990, pp. 1715–1721.

[3] Saito, K. Quintiere, J.G., and Williams, F.A., Fire Safety Science – Procs. the First International Symposium, Hemisphere Pub., 1985, pp. 75–86.

[4] Saito, K., Williams, F.A., Wichman, I.S., and Quintirere, J.G., **J. Heat Transfer**, 111:438 (1989).

[5] Quintiere, J.G., Harkleroad, M., and Hasemi, Y., **Combustion Science and Technology**, 48:191 (1986).

[6] Kulkalni, A.K., Kim, C.I., **Combustion Science and Technology**, 73:493 (1990).

[7] Delichatsios, M. and Saito, K., **Fire Safety Science – Procs. the Third International Symposium**, Elsevier Science Publishers Ltd., 1991, pp. 217–226.

[8] Williams, F.A., **Sixteenth Symp. (Intl) on Combustion**, The Combustion Institute, 1977, pp. 1281–1294.

[9] Williamson, R.B., Revenaugh, A., and Mower, F.W., **Fire Safety Science – Procs. the Third International Symposium**, Elsevier Science Publishers Ltd., 1991.

[10] Daikoku, M., Lin, W.X. and Saito, K., "Visualization of Fire–Induced Flow", Presented at **the Central State Section, The Combustion Institute**, Nashville, TN, April, 1991.

[11] Roseman, R., Han, C.Y., Wee, W.G., and Murphy, J., "Classification of Infrared Images using Pattern Recognition and Artificial Neural Networks", **Procs. the Symposium on Advanced Manufacturing**, University of Kentucky, Lexington KY, Sept. 1989.

[12] Lyons, V., and Gracia–Salcedo, C.M., "Determination of Combustion Gas Temperatures by Infrared Radiometry in Sooting and Nonsooting Flames", **NASA AVSCOM Technical Report** 88–C–008, 1989.

[13] Lin, W.X., **MSME thesis**, Department of Mechanical Engineering, University of Kentucky, Lexington, KY 40506, 1992.

[14] Megaridis, C.M., and Dobbins, R.A., **Twenty–second Symposium (Intl.) on Combustion**, The Combustion Institute, pp. 353–362.

[15] Saito, K., Williams, F.A., and Gordon, A.S., **Combustion Science and Technology**, 51:291 (1987).

[16] Yumoto, T., J. **Japanese Society of Safety Engineers** (in Japanese), 10:147 (1971).

[17] Katto, Y., **Heat Transfer** (in Japanese), Yokendo, Tokyo, 1977.

[18] A. K. Jain, **Procs. of IEEE**, 69 (3), 1981, pp.349–389.

[19] Arakawa, A., **MSPE Thesis**, Dept. of Precision Engineering, Tohoku University, Aoba–Aramaki, Sendai 980, 1980.

Figure Captions

Figure 1 (a) Experimental apparatus; (b) Image processing system.

Figure 2 The ratio of wall radiation to flame radiation as a function of flame emissivity with band–pass filters (5.0, 6.0, 8.0 and 10.6 μm with band–pass width $\pm$ 0.5 μm) and without filter. (top: wall temperature, T_{wall} = 600K and flame temperature, T_{flame} = 1100K; bottom: T_{wall} = 600K and T_{flame} = 1200K).

Figure 3 Wall temperature profiles measured using infrared imaging system with and without band–pass filter Left side column: results from passing through a methane–air diffusion flame; right side column: results without passing through the flame.

Figure 4 Color coded infrared images on a fire–heated wall. Top: a blue methane–air premixed flame with 80 W/cm^2 heat flux is used as fire source; and bottom: a 10cm diameter (sooty and yellow) hexane pool flame was used as a fire source. The images (a) and (c) are at a steady state condition, and were obtained through the flame using the 10.6 μm band–pass filter, (b) is at 1s after the burner was turned off, and (d) is at 4s after the flame was quenched.

Figure 5 (a) The horizontal (X) and vertical (Z) locations of a 100 ^{o}C isotherm on a fire–heated Marinite wall; (b) Progress rate of a 100^{o}C isotherm, V_{100}, in horizontal (X) and vertical (Z) directions as a function of time.

Figure 6 Color coded infrared images for upward flame spread along vertical (made of black cardboard) corner walls. Top: infrared images obtained using a infrared camera with a band–pass filter 10.6$\pm$0.5μm every 20s after ignition, and bottom: video camera images obtained at the corresponding time periods to the infrared images.

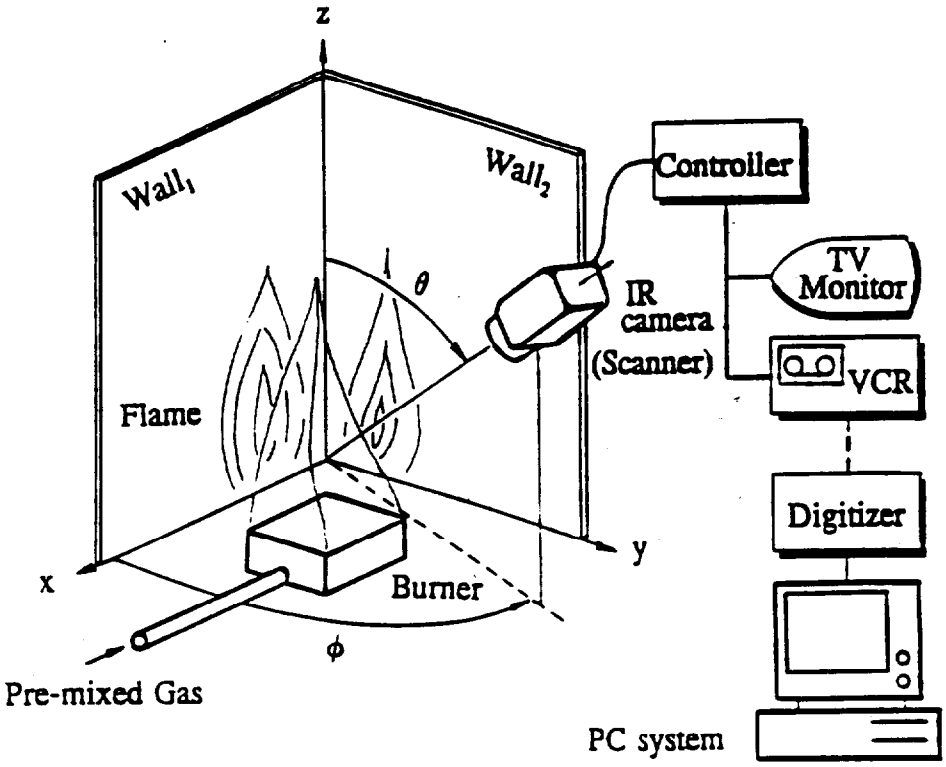
z
Wall1
Wall2
θ
Flame
x
y
Burner
ϕ
Pre-mixed Gas
Controller
TV Monitor
IR camera (Scanner)
VCR
Digitizer
PC system

(a)

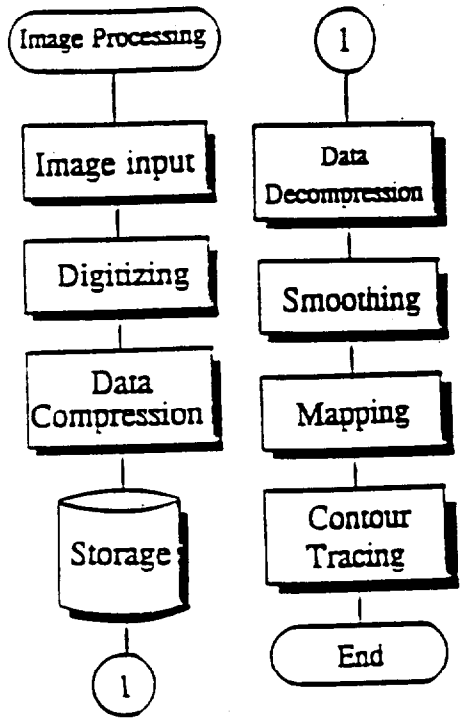
Image Processing
Image input
Digitizing
Data Compression
Storage
1
1
Data Decompression
Smoothing
Mapping
Contour Tracing
End

(b)

Fig. 1

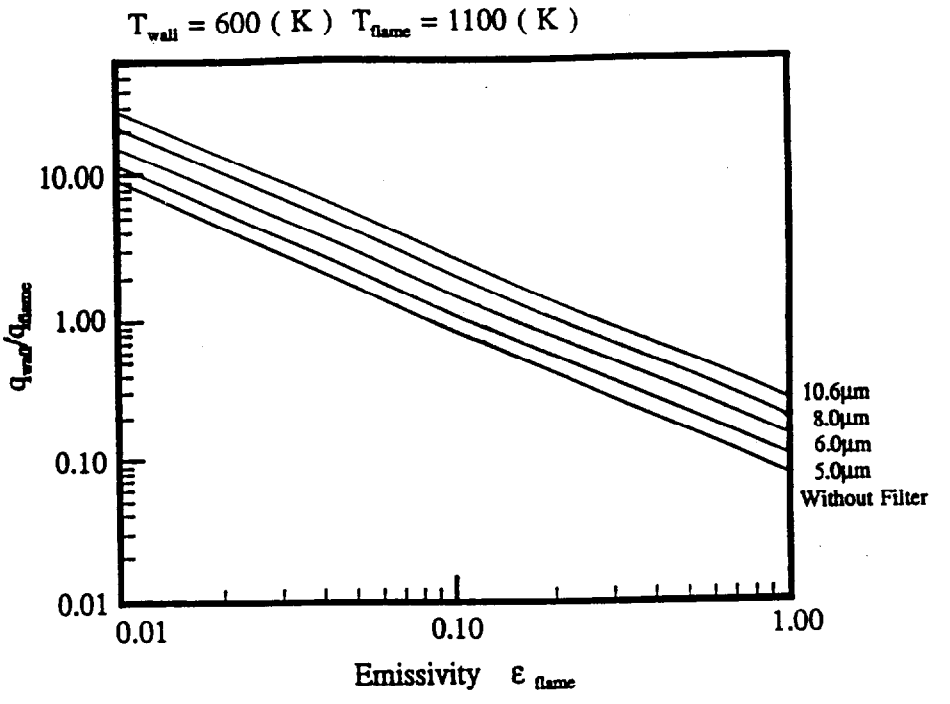
T_{wall} = 600 (K) T_{flame} = 1100 (K)
10.00
1.00
0.10
0.01
q_{wall}/q_{flame}
0.01
0.10
1.00
Emissivity ε_{flame}
10.6μm
8.0μm
6.0μm
5.0μm
Without Filter

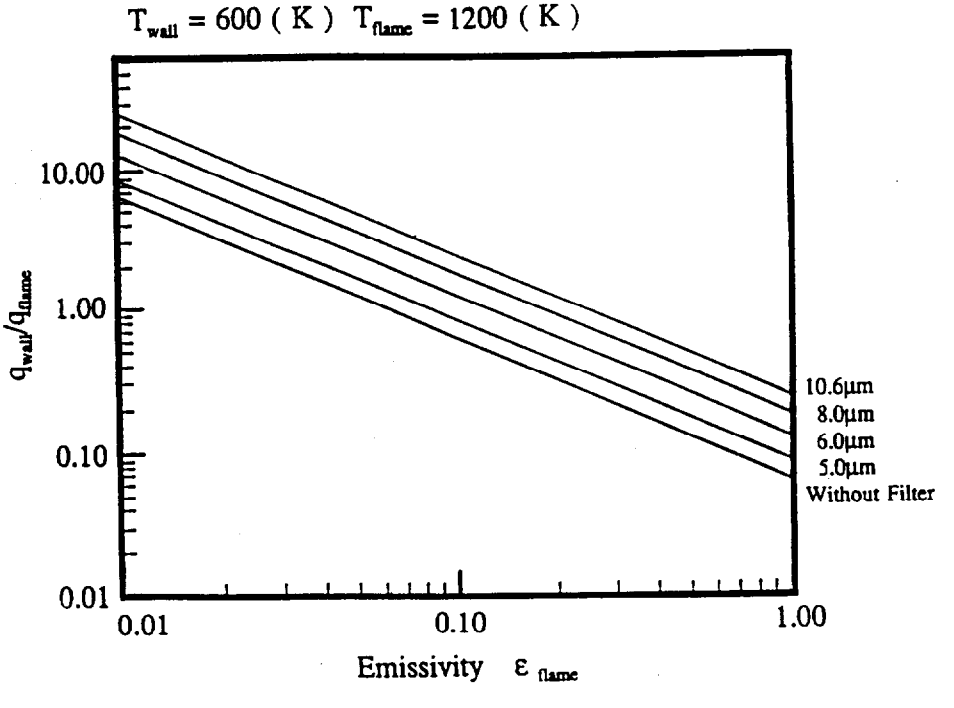
T_{wall} = 600 (K) T_{flame} = 1200 (K)
10.00
1.00
0.10
0.01
q_{wall}/q_{flame}
0.01
0.10
1.00
Emissivity ε_{flame}
10.6μm
8.0μm
6.0μm
5.0μm
Without Filter

Fig. 2

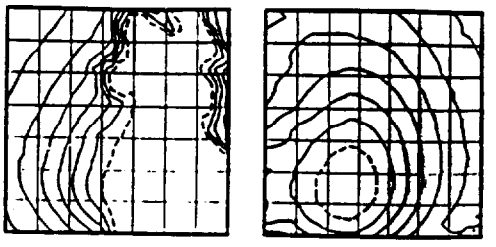

(a) Without Filter

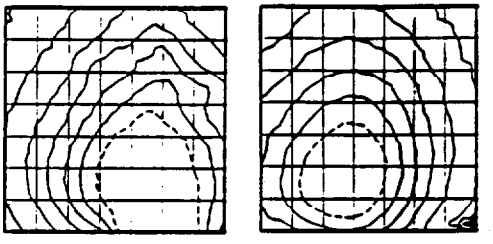

(b) Using 10.6μm Filter

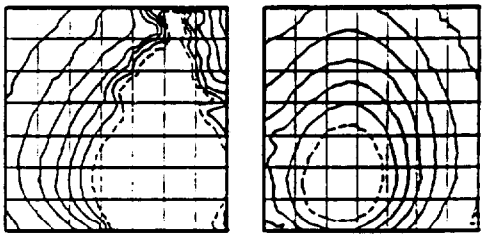

(c) Using 8.0μm Filter

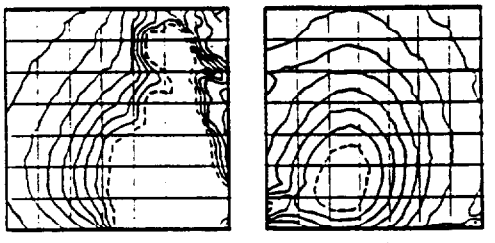

(d) Using 6.0μm Filter

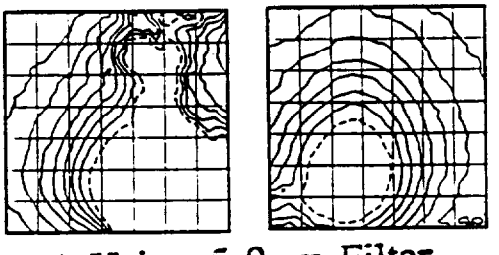

(e) Using 5.0μm Filter

Fig. 3

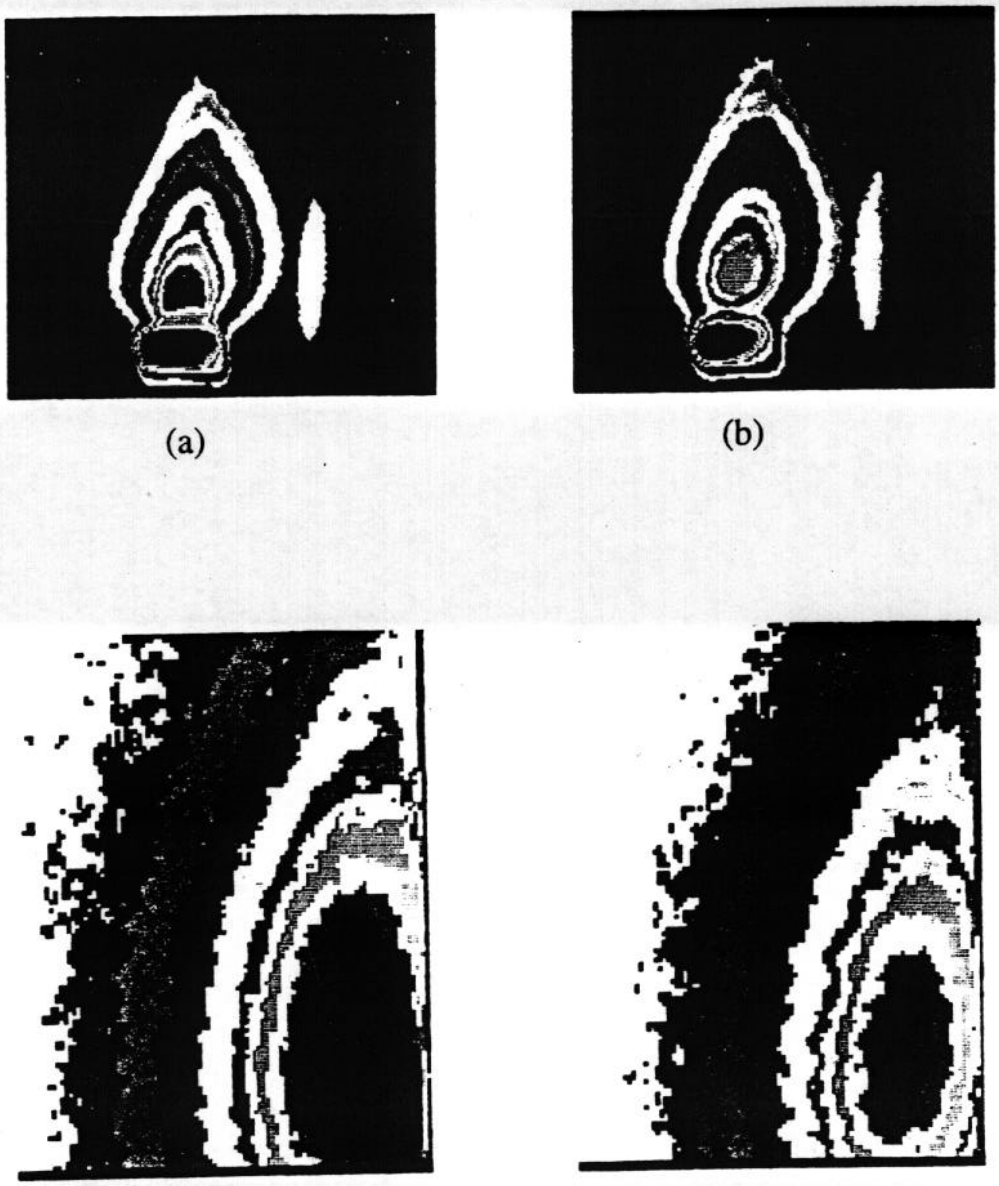

Fig. 4

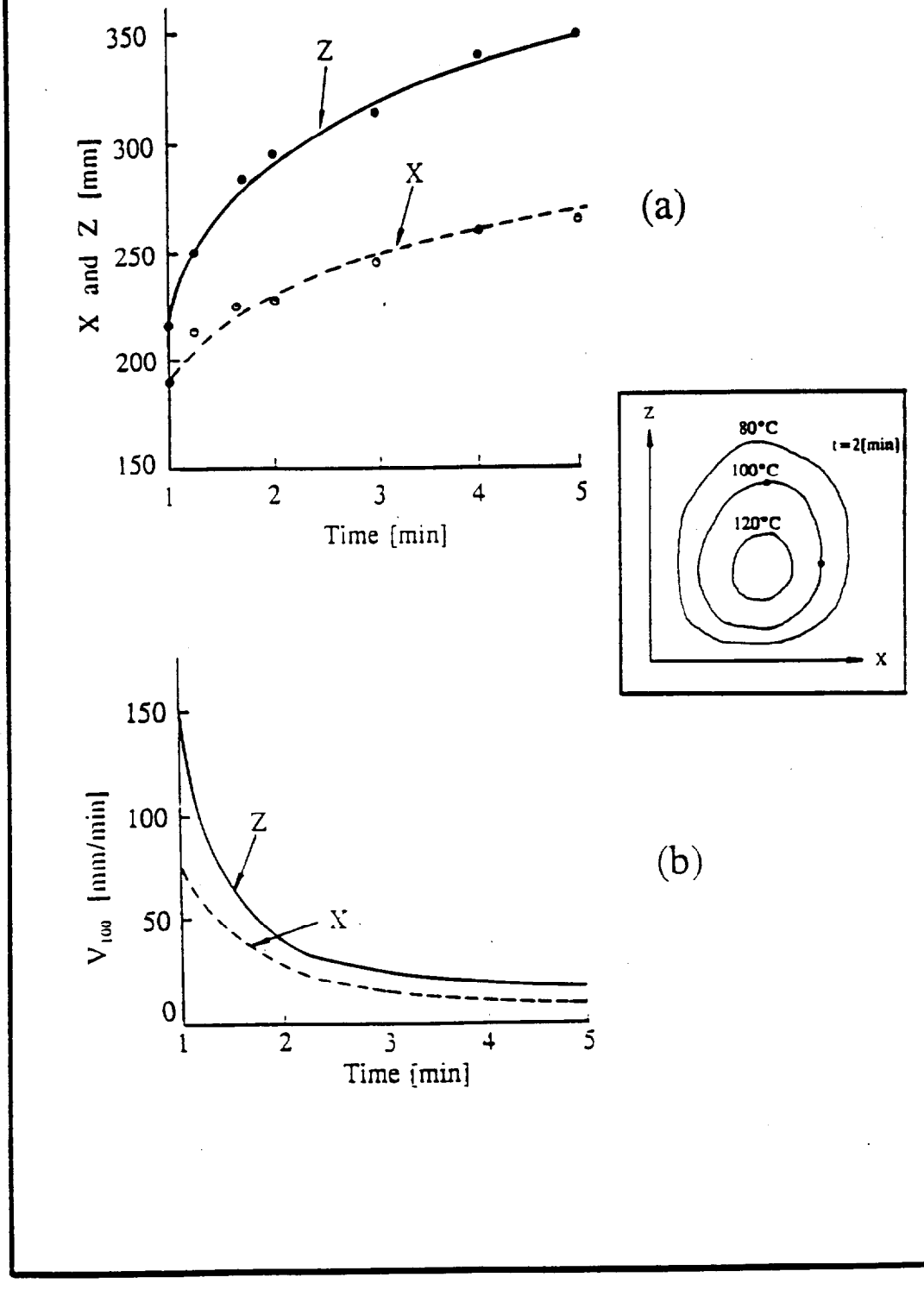
350
300
250
200
150
X and Z [mm]
Z
X
(a)
1
2
3
4
5
Time [min]
Z
80°C
t=2[min]
100°C
120°C
X
150
100
50
0
V_{100} [mm/min]
Z
X
(b)
1
2
3
4
5
Time [min]

Fig. 5

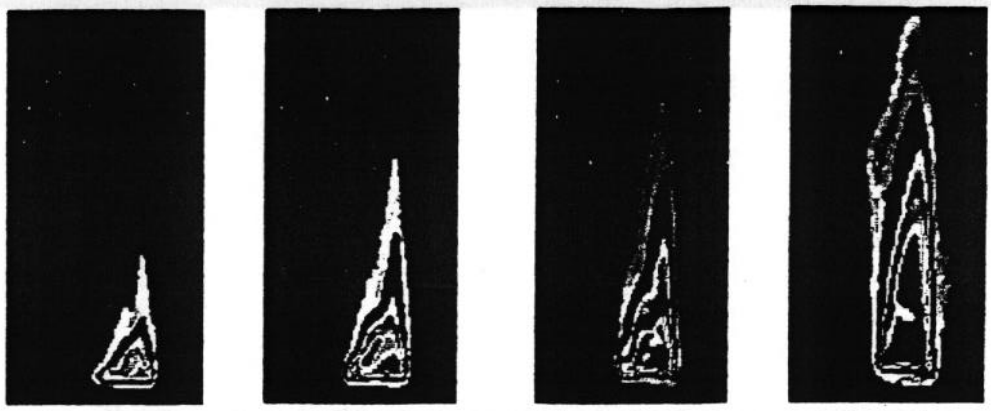

Temperature (K)

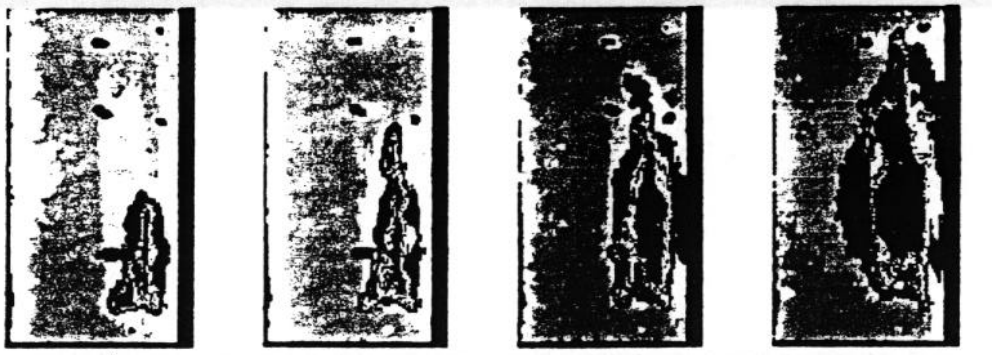

Relative Intensity

Fig. 6

First Asian Conference on Fire Science and Technology
October 9-13, 1992, University of Science and Technology of China
Hefei, Anhui, P.R. China.

ACFST-B-19

FIRE-INDUCED FLOW ALONG THE VERTICAL CORNER WALL

Cheng Qian *, Kozo Saito **
(Mechanical Engineering Department,University of Kentucky,
Lexington, Kentucky 40506-0108, U.S.A.)

ABSTRACT

Upward flame spread along the vertical corner wall is a severe phenomenon due to its rapid spread rate in building fires. We conducted this study to investigate what kind of flow will be developed along the vertical corner wall by fires using a room corner model and placing a square gas burner on the floor. The parameter changed is the location of the burner respect to the walls. After a steady state condition was achieved, stream lines were visualized by particles illuminated by a laser sheet, and recorded by a 35mm camera. Results revealed that the oscilation of the flame, the long-range action of the turbulent plume and the swirl produced under some condertions are critical elements for understanding of turbulent entraiment and flame spread processes of the room corner fire.

KEYWARDS: Compartment Fire; Fire Spread; Fire Plume.

INTRODUCTION

Turbulent upward flame spread along a vertical wall has been studied intensively in our previous work [1]. The upward flame spread along the vertical corner wall, however, is not well understood, in spite of the fact that the phenomenon is an important subject in fire safety due to rapid spread rate and high intensity radiant emmission from flame and burning walls. This is because of the lack of understanding of turbulent entrainment and turbulent mixing processes in corner fires. Experimental data and prediction model are largely limited to axisymmetric flames and plumes in an open environment. Limited information is available for flames against a wall or in a corner of two walls. The techniques of flow visualization have been used with some notable success in studing the coherent structures of turbulent flows in recent years. In the previous study, smoke streak lines were used to visualize flow patterns; some vortex characteristics of the fire-induced flow were revealed [2]. In the present experiment, instantaneous stream lines were visualized by particle track method that can lead to a quantitative visualization by PIV(Particle Image Velocimetry) technique in the next step. To understand the transient nature of fire spread, it may be useful and necessary to understand the simpler steady state scenario. Thus, in this study, visualization of steady fire-induced flow along the corner wall is conducted and characteristics of the flow are discussed.

EXPERIMENTAL METHOD

A schematic of the experimental apparatus is shown in Fig.1. The walls are made of Marinite boards(noncombustible/heat insulating material) with 2cm thickness which are backed up by 1.5cm thickness particle board for heat insulation and are fixed on a steel frame. Each of the two walls is 1.6m in height and 1.0m in width. A square gas burner whose exit dimension is 0.15x0.15m was placed on a corner of floor. The level of floor was the same as the burner exit to eliminate flow disturbances by the burner. Blue propane-air premixed flames were

used for flow visualization to suppress the emission from soot and to obtain clear visualization results. The heat release rate of the burner was changed up to 22.5kW. It was found that the heat release rate is a weak parameter to influence fire-induced flow. Hence experiments were performed by changing the burner stand-off distances(x,y) as shown in Fig.1, and the heat release rate was fixed at 6.0kW. The 50% intermittent flame height that is defined as the average of flame tip and continuous flame height is about 0.25m [3]. Ambient air was seeded with a few micron magnesium oxide particles. These particles can float in the air approximately 5 minutes following the flow faithfully. A 5 watt argon-ion laser was used to produce a sheet of laser light that slices through the plume region of the fire vertically and horizontally. Tracing particles are illuminatted by the laser sheet and the instantaneous flow stream lines were visualized and recorded by a still camera with a shutter speed 1/8 s. The location of the laser sheet is determined from the equation of the plane in which the laser sheet lies.

RESULTS AND DISCUSSION

1.Turbulent Characteristics

The flow visualization photographs presented in Fig.2 clearly show the complex turbulent flow field. As is well known, the transition of laminar flame to turbulent occurs with increasing velocity and scale. At the same time, the luminous height of the buoyancy-contralled flame begins to oscillate. This oscillation is due to the aerodynamic instability caused by the interference between the flame and the surrounding air [3]. These fluctuation dominated turbulent entrainment; turbulent mixing processes are shown in side view photoghaphs in Fig.2(a), (b), (c) and (f). We found that the air flow already becomes non-uniform with the fluctuation in velocity before it enters into the plume, even it is far away from the plume. The velocity fluctuation as a function of time is shown in Fig.2(a), (b) and (c), and distorted stream lines are shown in Fig.2(c) and (d). Hence the turbulent fluctuations generated in the plume area are not only carried away in down stream(by convection) but also transferred normal to the stream lines, and not only directly in adjacent layers of fluid(by diffusion) but also over a great distance. This phenomenon is so called "long-range action" of the turbulence [5]. Note that the turbulence long-range action is not only in the transverse direction, but also becomes important in reverse direction in a low speed flow field, like the natural convection induced by fires. The long-range action may be attributed to the transmission of pressure fluctuation over a distance.

2.Vortex Characteristics

Swirl formation is another important feature in the fire-induced flow along vertical corner walls. A non-symmetric location of the burner respect to the walls would produce a large swirl around the flame which could change the entrainment rate significantly [2,6]. Photographs in Fig.2(d), (e) and (g) show the instantaneous stream lines in a horizontal section for three different locations of the burner. Some representative flow patterns of the induced convection current around the plume are shown in Fig.3. In vertical section the flow pattern(Fig.3(a)) is similar to that of the flow field induced by a turbulent jet from a floor [7]. When the two edges of the burner are flush with the corner walls, the plume will attach itself to the walls. The plume in the corner can be thought of as one quarter of a free plume, four times as strong, shown in Fig.3(b). In an idealized situation the entrainment rate of a fire plume placed in a corner will only be a quarter of that of the four times stronger plume placed far from a wall. When the burner is moved away from the walls, a couple of vortices are found at two edge of the burner, see Fig.2(g) and Fig.3(c). When the burner is closer to or flush with one wall, one of the vortices bocomes stronger and dominates the induced current in the corner(see Fig.3(d)). A side part of the flame is detached from the main body by the axial flow of the vortex as shown in Fig.2(e)-(f). But the breakdown of the vortex occurs quickly after it was produced.

SUMMARY

The flow visualization experiments resulted in the following conclusions: (1)The oscillation of the flame and the long-range action of the turbulent plume phenomena are important in air entrainment of corner fires because the constrains of the air entrainment by the presence of the walls. (2)A non-symmetry location of the burner respect to the walls likely produces a vortex at one edge of the burner. The vortex with a strong axial flow that detach the flame may enhance the flame spread rate largely. Hence the oscillation of the flame, the long-range action of the turbulent plume and the swirl in the flame are critical elements for understanding of turbulent entrainment and turbulent mixing processes in a room corner fire. (3)The flow process is novel and warrants further investigation. This work was supported by NIST grant #60NANB1D1142.

REFERENCES

1. K. Saito, J.G. Quintiere and F.A. Williams, Fire Safety Science-Proceedings of the First International Symposium, Hemisphere, (1985),75.
2. M. Daikoku, W. Lin and K. Saito, The Central States Section,The Combustion Institute Meeting, (1991 Spring), 237.
3. G. Heskestad, Fire Safety Journal, Vol.5(1983),109.
4. H.Ishida, Fire Safety Journal, Vol.18 No.3(1992),213.
5. G.N.Abramovich, Recent Developments in Theoretical and Experimental Fluid Mechanics, Springer-Verlag, Berlin Heidelberg New York(1979), 467.
6. E.N.Tangren, W.S.Sargent and E.E.Zukoski, NSF Grant ENV76-06660 and U.S. Dept. of Commerce, Nat. Bur. of Stand. Grant5-9004, California Institute of Technology, Pasedena, CA, June 1978.
7. M.V.Dyke, An Album of fluid Motion, The Parabolic Press, Stanford, California(1982), 99.

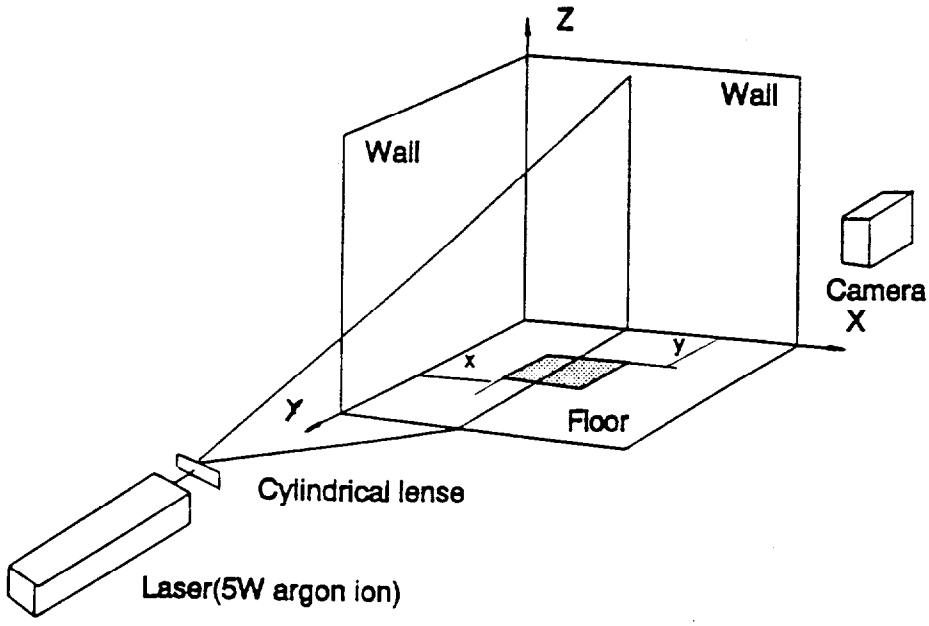

Fig.1 Schematic of the illumination and coordinate system for the model of room corner fire

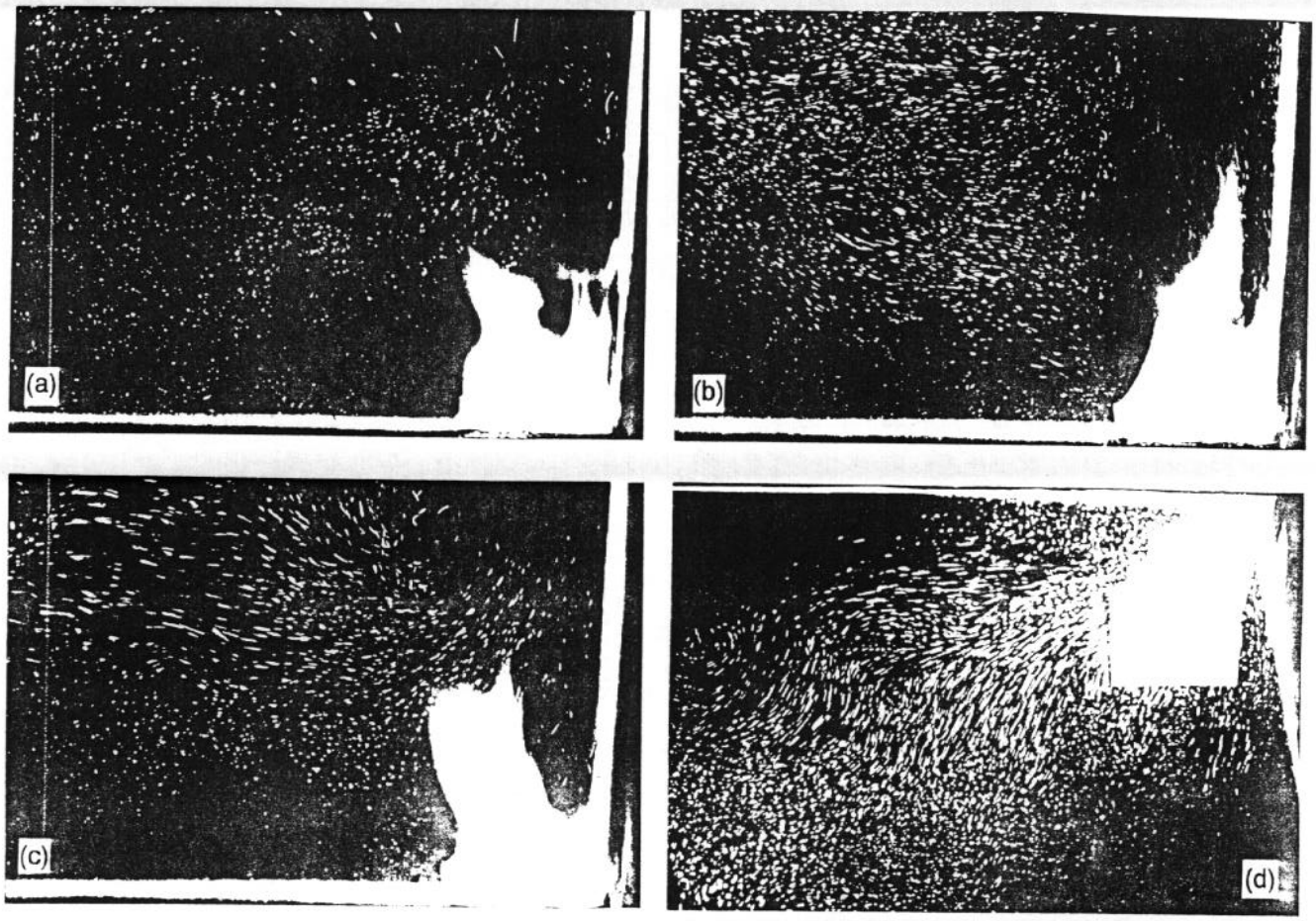
(a)
(b)
(c)
(d)

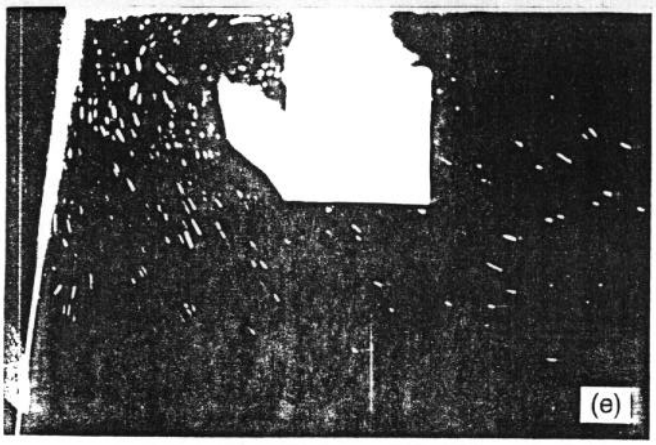

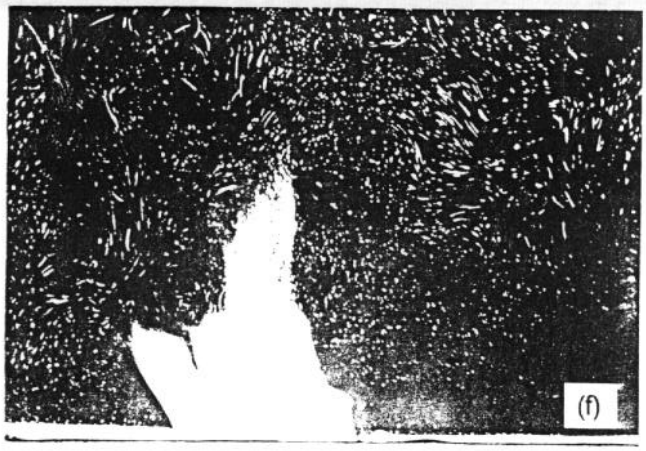

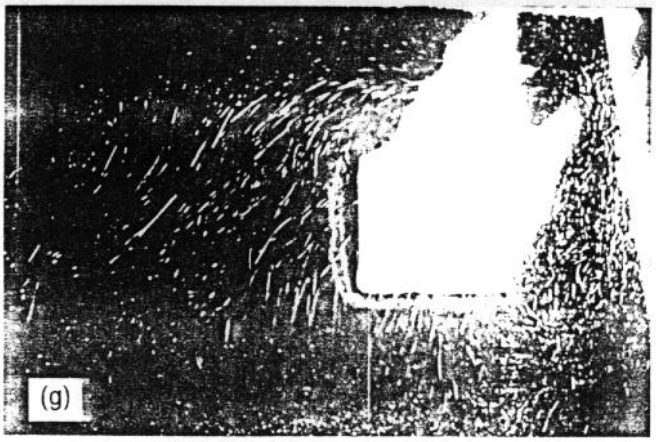

[illegible] instantaneous [illegible]
[illegible] section [illegible]
distance [illegible]

Fig.(2)	Stand-off(M) x	y	Section illuminated by laser sheet (M)
(a),(b),(c)	0.0	0.0	z=0.075
d)	0.0	0.0	z=0.150
[illegible]	0.0	[illegible]	[illegible]
[illegible]	0.0	[illegible]	[illegible]
g)	0.1	[illegible]	z=0.150

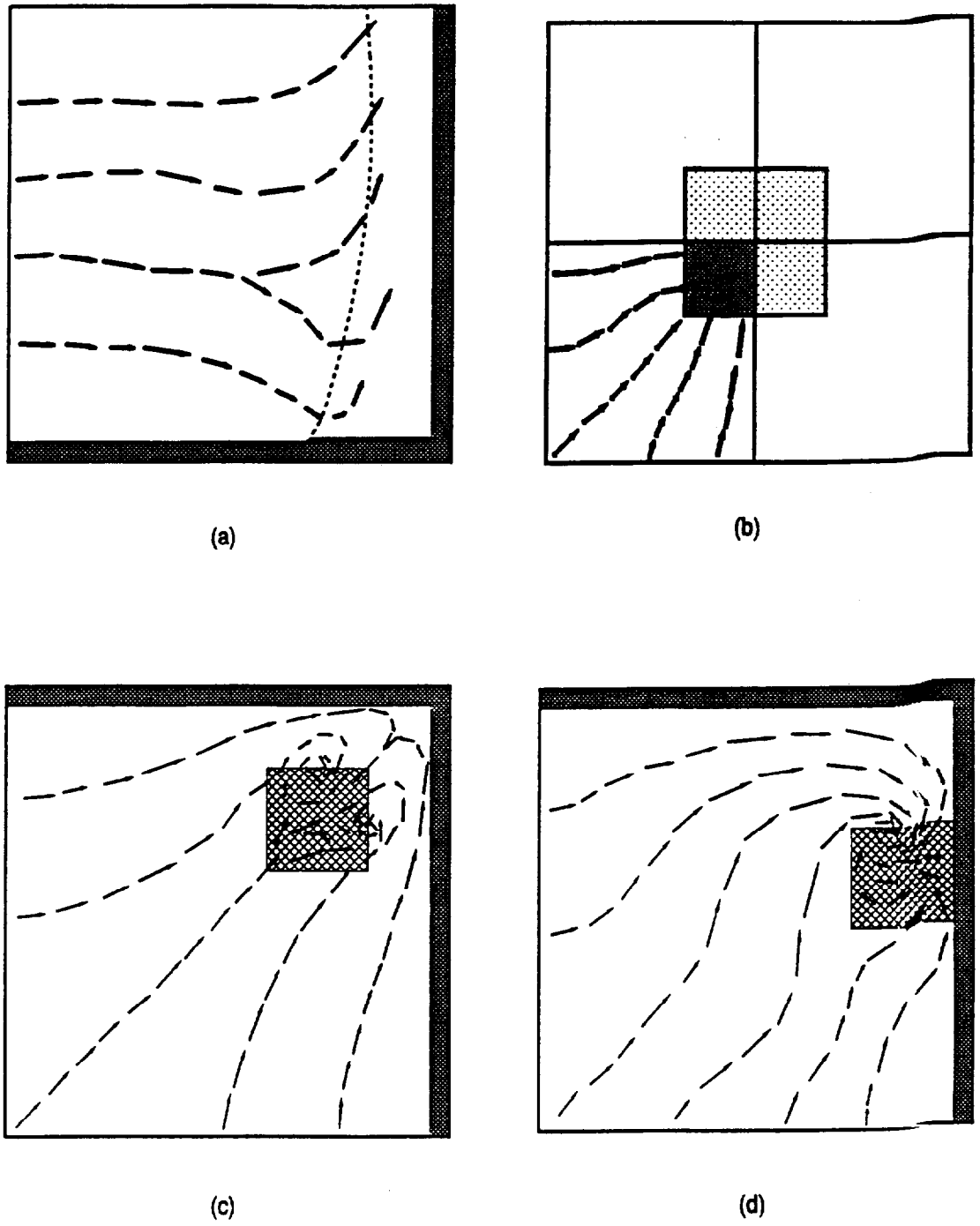

Fig.3 Typical flow patterns: (a) vertical section, (b) quarter model for a corner plume, (c) and (d) horizontal sections.

APPENDIX – A

Measurements of Temperature Distribution and Heat Flux at a Vertical Corner Wall Surface

The one–half scale room corner model was used for this measurement. A propane–air premixed flame was established on a square floor burner whose exit surface area is 15 cm x 15 cm to heat the Marinite–made corner walls. After a steady state temperature distribution was established on the wall surface, the temperature distribution was measured with 100 μm diameter Chromel–Alumel thermocouples as a function of burner heat release rate and burner stand–off distance at eighteen different locations as shown in Fig. 1. The thermocouples were placed approximately 1 mm below the Marinite wall surface by drilling a small holes and fixing the thermocouples by an organic glue. The thermocouple beads were then covered by pressing Marinite powder to prevent direct exposure of radiation from the flame and convection heat. Thermocouple readings were recorded in a computerized data acquisition system which can record the eighteen signals less than 100 μs. These thermocouple readings confirmed that the wall temperature achieved a steady state temperature distribution within 30 minutes after the burner was on. All the measurements reported here were obtained after a steady state temperature distribution was established on the wall.

Typical temperature measurement results are shown in Figs. 2a through 3e; and vertical and horizontal temperature distributions along the wall are plotted respectively in Figs. 4 and 5 for the burner heat release rate, 13.5 kW and the burner stand–off distances 2.5 and 5 cm.

Total heat flux was measured using water cooled heat flux meters at the same eighteen locations as the thermocouple measurements after the wall surface temperature achieved a steady state condition. The results for twelve different conditions are shown in

Figs. 6a through 8d. To check the reproducibility of the data, the measurements were repeated three times at three different conditions and twice at the other conditions. The reproducibility is higher than 90 %. in each location.

Figure Captions

Fig. 1 Measurement location for temperature and heat flux at the vertical corner wall surface. Numbers in figure is in centimeter.

Fig. 2a Steady state temperature distribution measured with Chromel–Alumel thermocouples. Propane–air premixed flame was established on a square floor burner whose exit area 15 x 15 cm. Burner heat release rate, Q (kW) = 9; and burner stand–off distance, BSD (cm) = 2.5. For all the experiments, the burner was placed in a symmetrical location.

Fig. 2b Q = 9 kW; and DSD = 5 cm.

Fig. 3a Q = 13.5 kW; and BSD = 0.

Fig. 3b Q = 13.5 kW; and BSD = 2.5 cm.

Fig. 3c Q = 13.5 kW; and BSD = 5 cm.

Fig. 3d Q = 13.5 kW; and BSD = 10 cm.

Fig. 3e Q = 13.5 kW; and BSD = 15 cm.

Fig. 4 Vertical temperature distribution along the wall at horizontal distance, 12.5 cm from the corner with Q = 13.5 kW and BSD = 2.5 and 5 cm.

Fig. 5 Horizontal temperature distribution along the wall at height, 15 cm with Q = 13.5 kW and BSD = 2.5 and 5 cm.

Fig. 6a Total heat flux distribution at the vertical corner wall with Q = 9 kW and BSD = 0.

Fig. 6b Q = 9 kW; and BSD = 5 cm.

Fig. 6c Q = 9 kW; and BSD = 10 cm.

Fig. 6d Q = 9 kW; and BSD = 15 cm.

Fig. 7a Q = 13.5 kW; and BSD = 0.

Fig. 7b Q = 13.5 kW; and BSD = 5 cm.

Fig. 7c Q = 13.5 kW; and BSD = 10 cm.

Fig. 7d Q = 13.5 kW; and BSD = 15 cm.

Fig. 8a Q = 18 kW; and BSD = 0.

Fig. 8b Q = 18 kW; and BSD = 5 cm.

Fig. 8c Q = 18 kW; and BSD = 10 cm.

Fig. 8d Q = 18 kW; and BSD = 15 cm.

Fig. 9 Vertical heat flux distribution along the corner wall at horizontal distance, 12. 5 cm from the corner with Q = 13.5 kW and BSD = 2.5 and 5 cm.

Fig. 10 Horizontal heat flux distribution along the corner wall at height, 15 cm with Q = 13.5 kW and BSD = 2.5 and 5 cm.

Fig. 11 Horizontal heat flux distribution along the corner wall at height, 35 cm with Q = 13.5 kW and BSD = 2.5 cm.

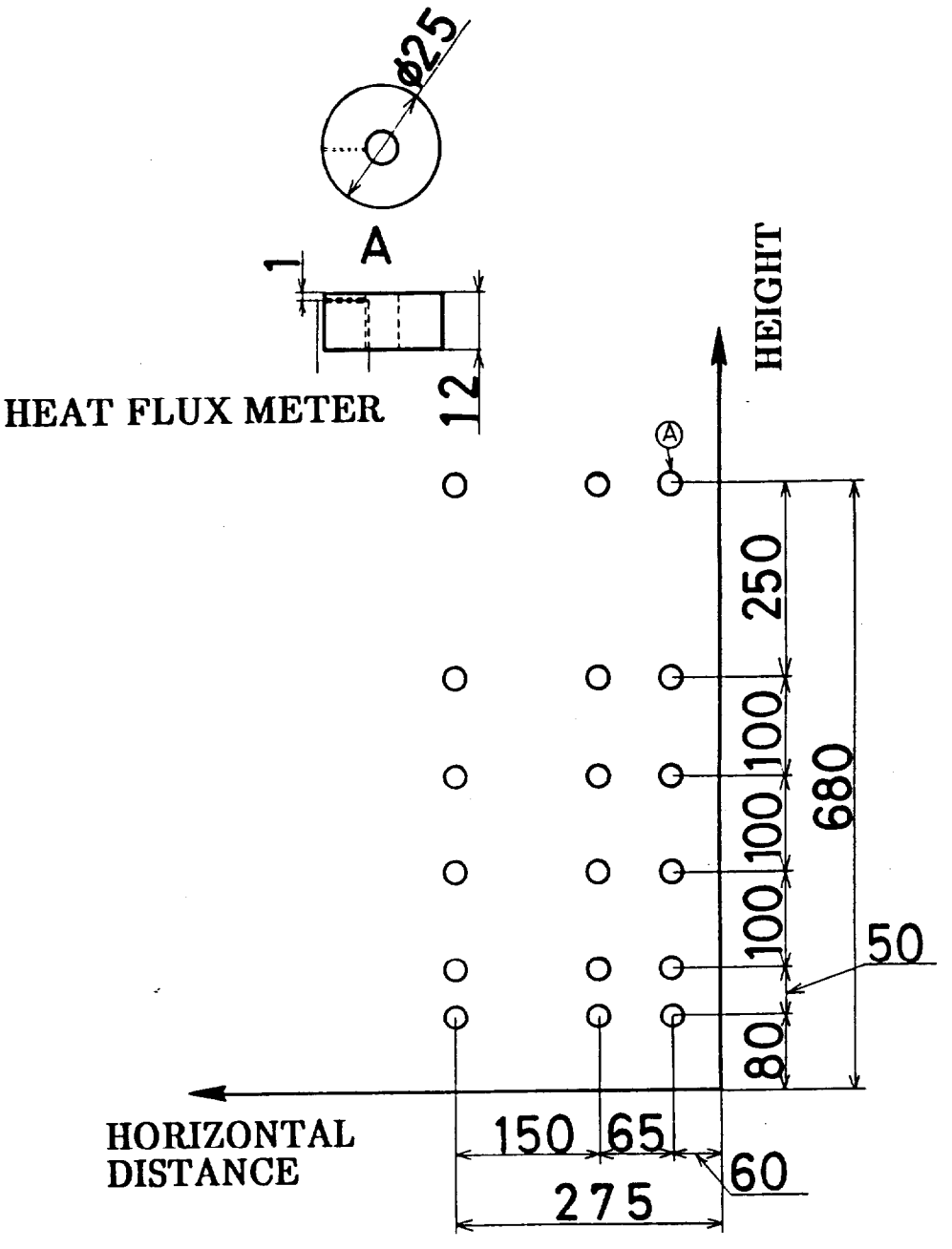
ø25
A
1
12
HEAT FLUX METER
HEIGHT
A
250
100
100
100
680
50
80
HORIZONTAL
DISTANCE
150
65
60
275

Fig. 1

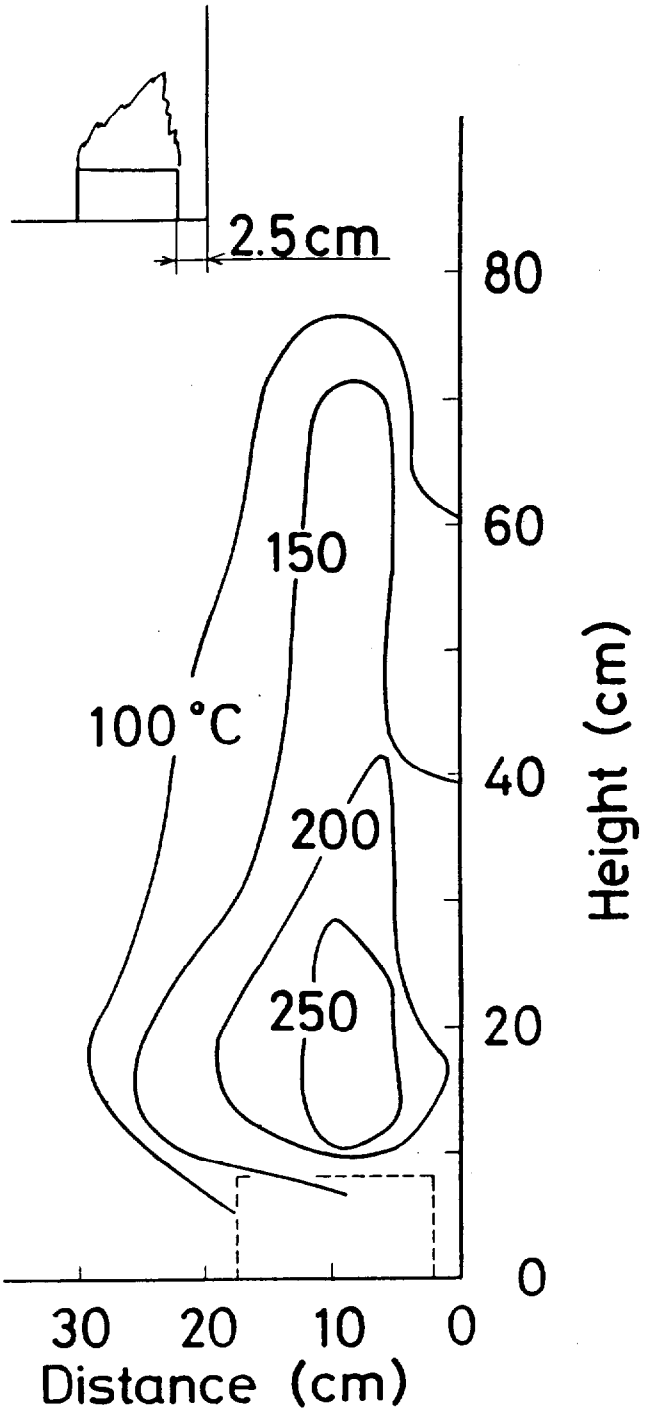
2.5cm
80
60
40
20
0
150
100 °C
200
250
Height (cm)
30
20
10
0
Distance (cm)

Fig. 2a

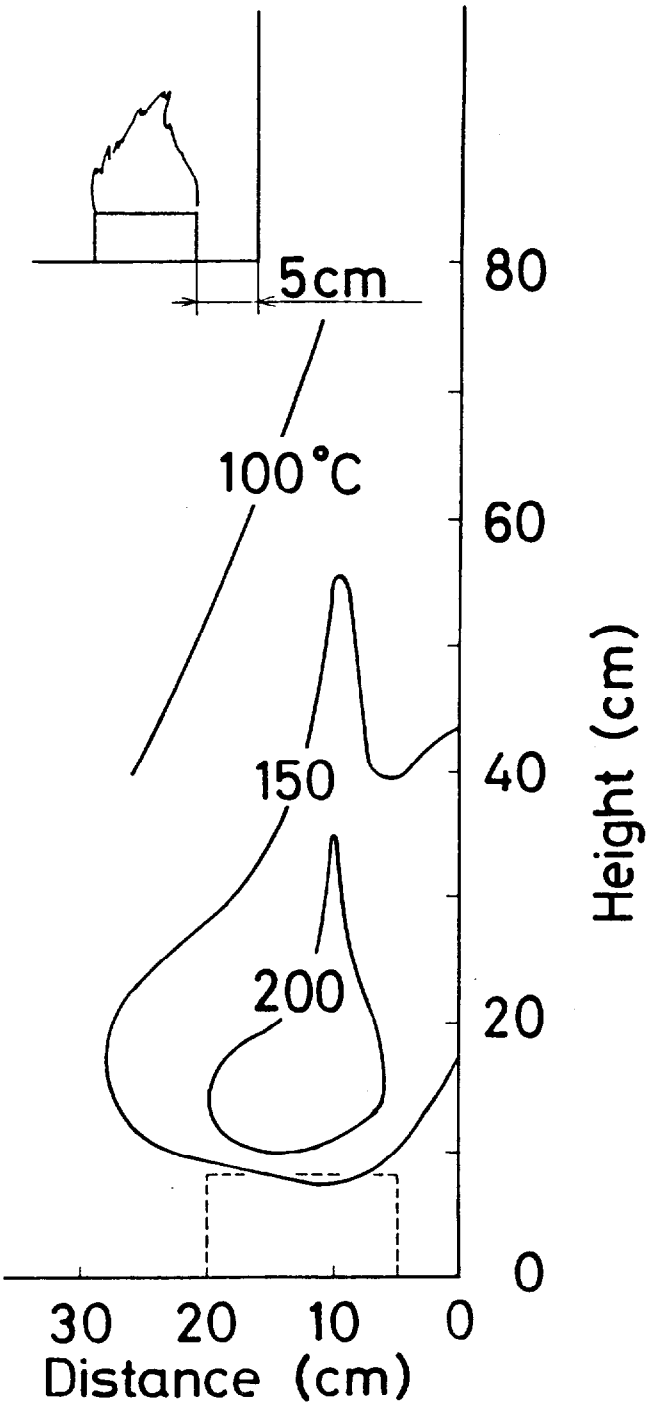

Fig. 2b

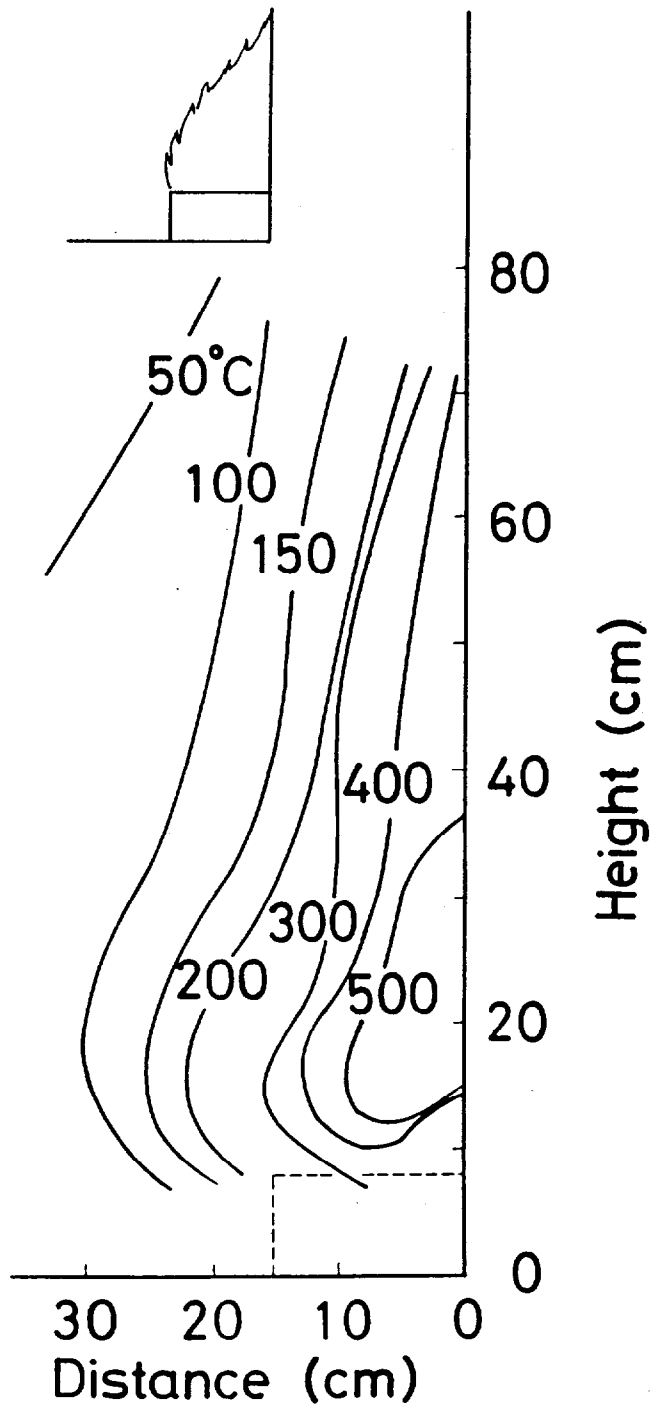
50°C
100
150
200
300
400
500
80
60
40
20
0
Height (cm)
30
20
10
0
Distance (cm)

Fig. 3a

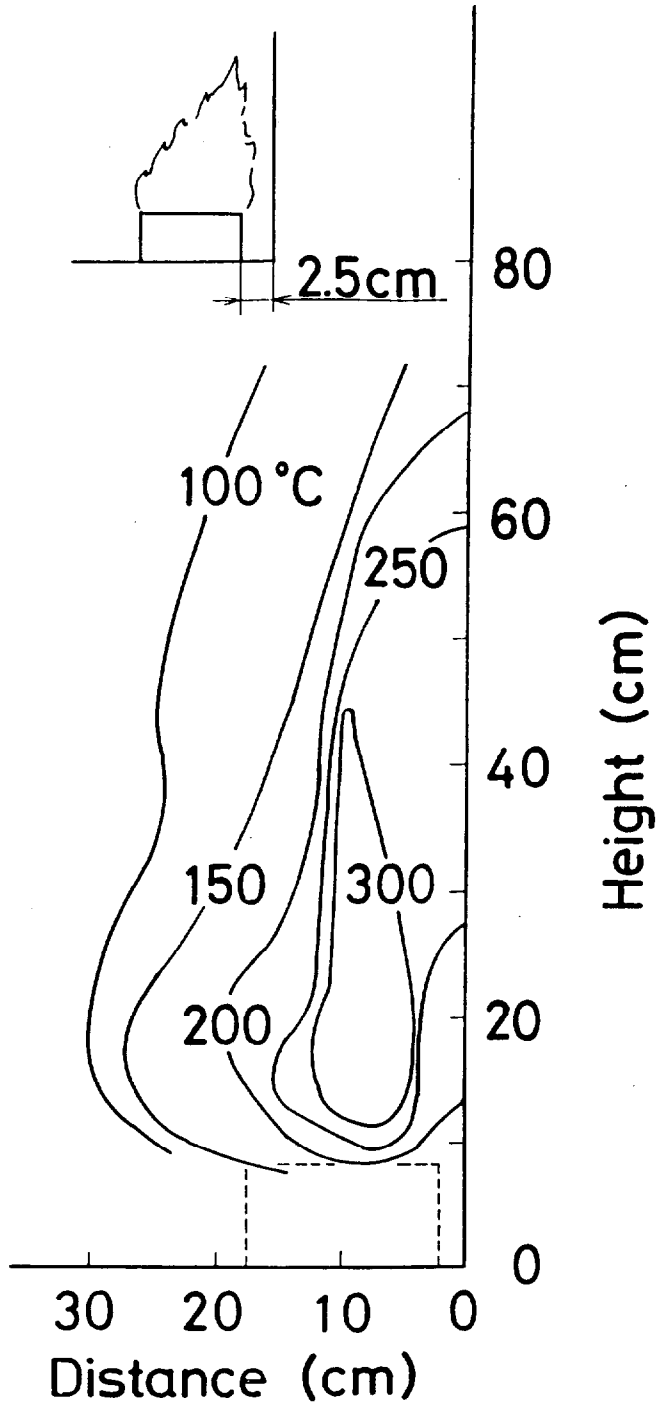
2.5cm
100 °C
250
150
300
200
80
60
40
20
0
Height (cm)
30
20
10
0
Distance (cm)

Fig. 3b

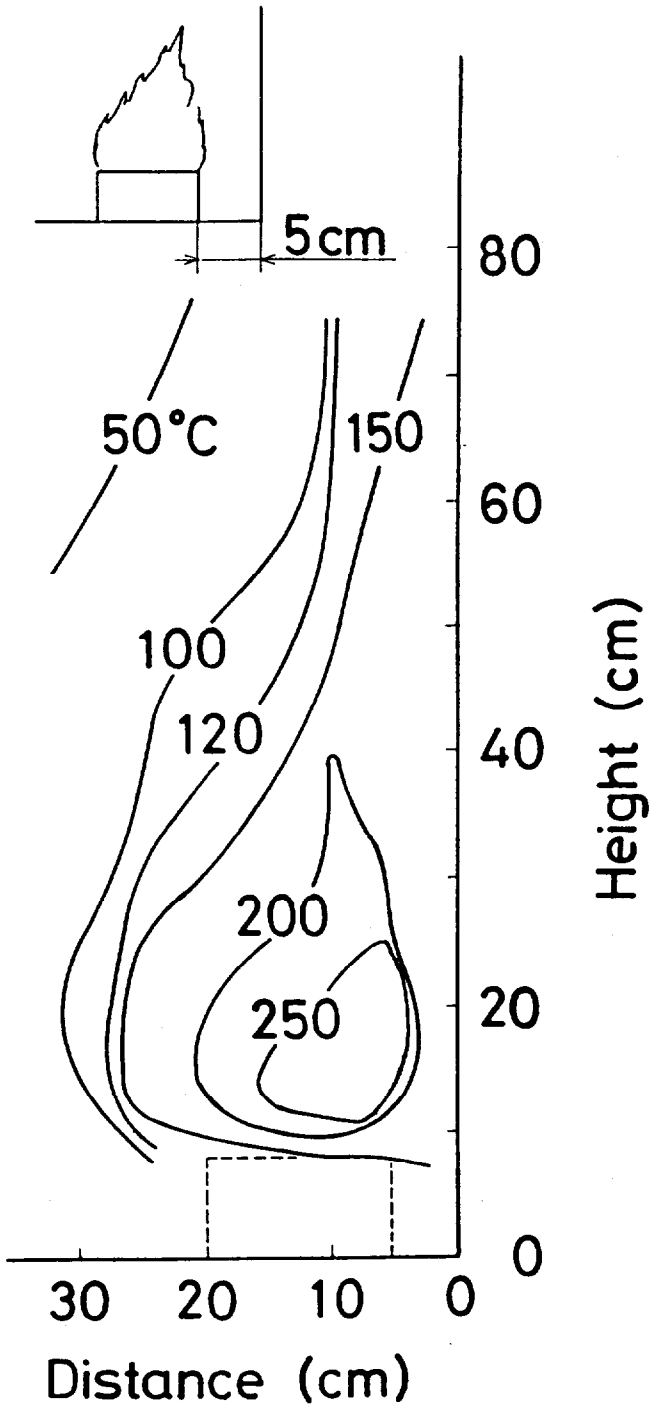
5cm
50°C
150
100
120
200
250
80
60
40
20
0
Height (cm)
30
20
10
0
Distance (cm)

Fig. 3c

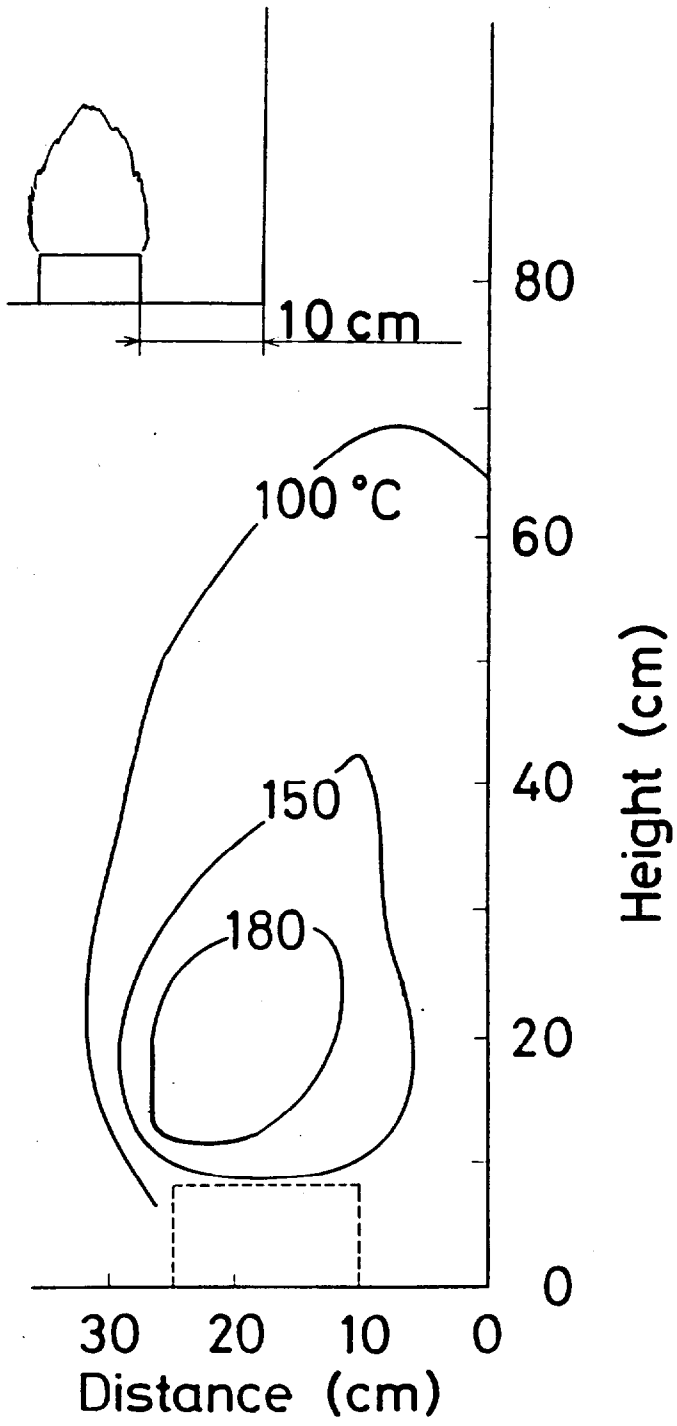

Fig. 3d

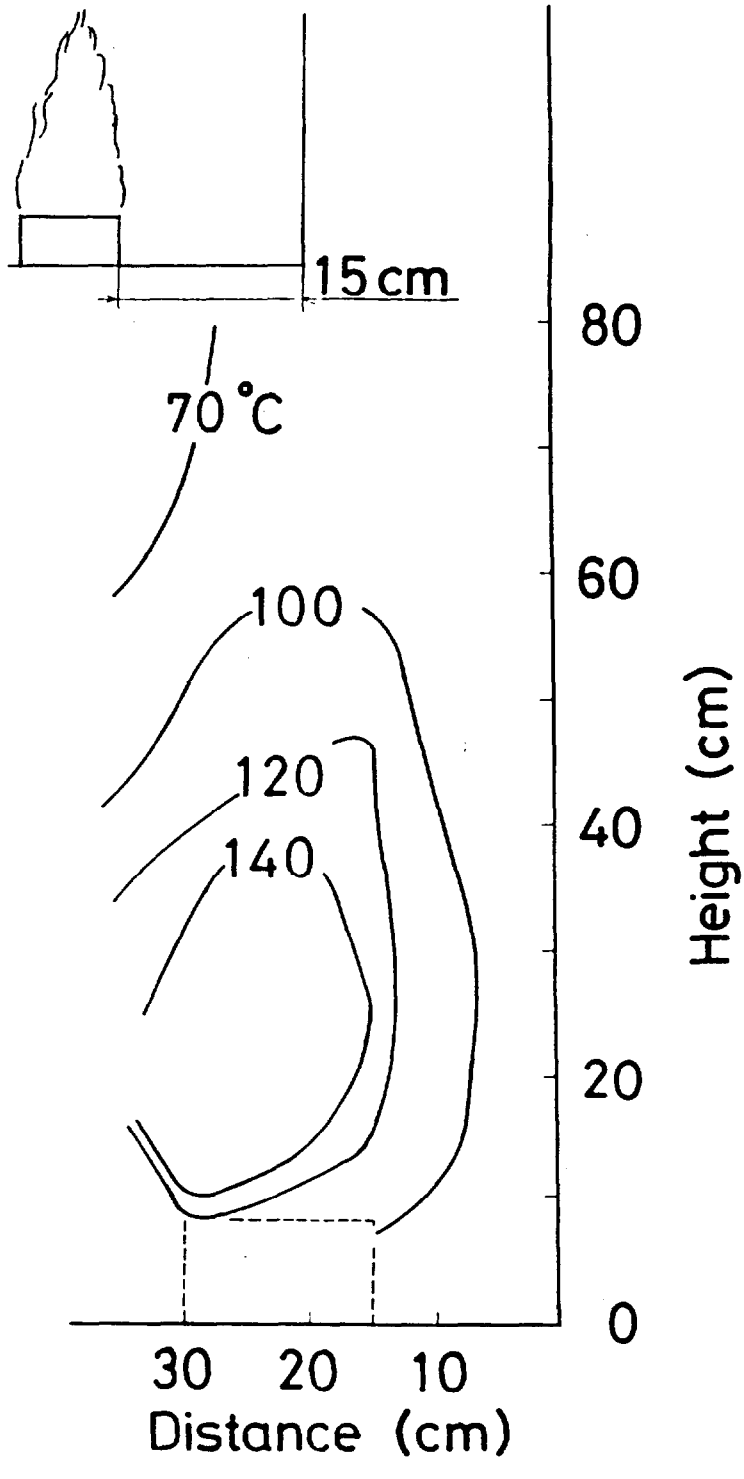

Fig. 3e

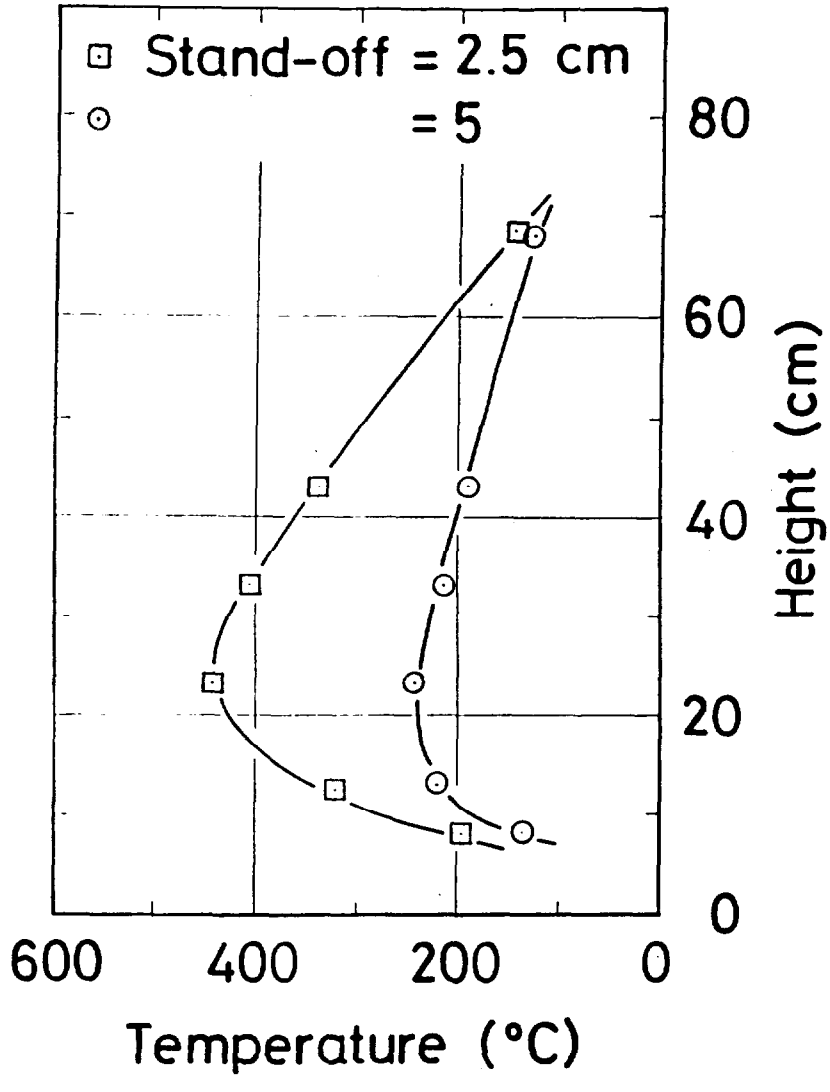
Stand-off = 2.5 cm
= 5
80
60
40
20
0
Height (cm)
600
400
200
0
Temperature (°C)

Fig. 4

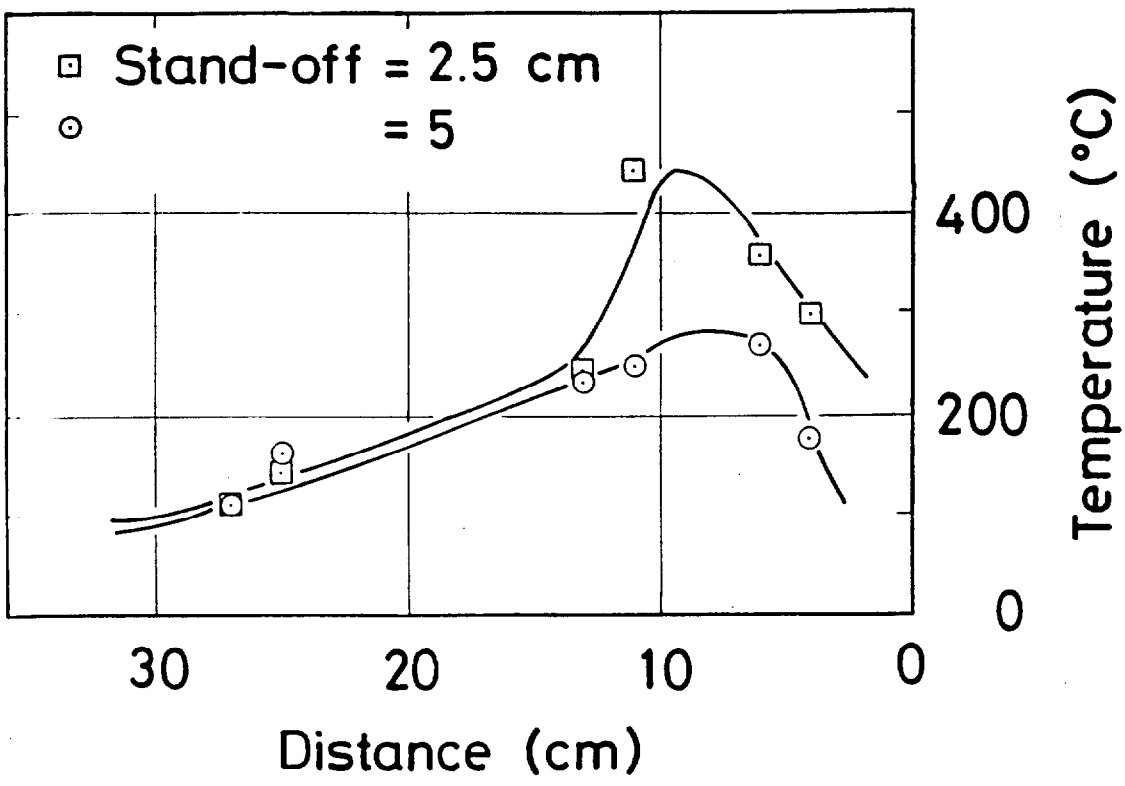

Fig. 5

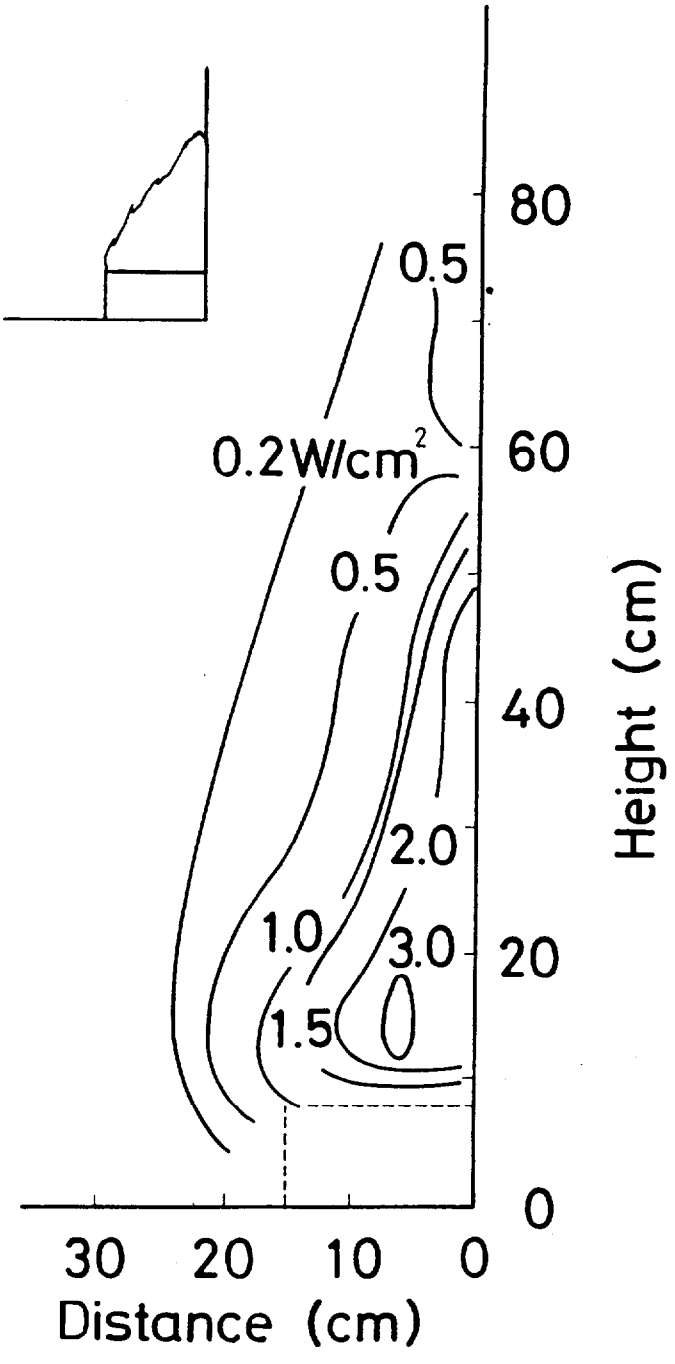
80
60
40
20
0
0.5
0.2W/cm²
0.5
2.0
1.0
3.0
1.5
Height (cm)
30
20
10
0
Distance (cm)

Fig. 6a

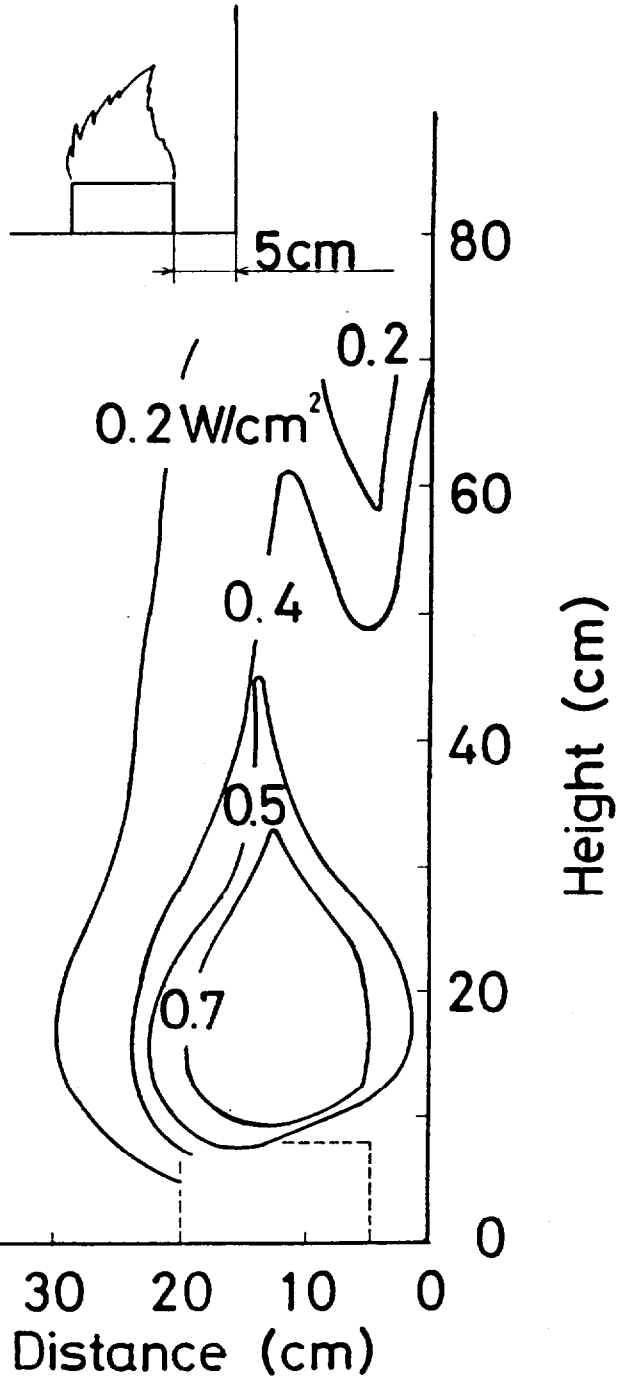
5cm
0.2
0.2W/cm²
0.4
0.5
0.7
80
60
40
20
0
Height (cm)
30
20
10
0
Distance (cm)

Fig. 6b

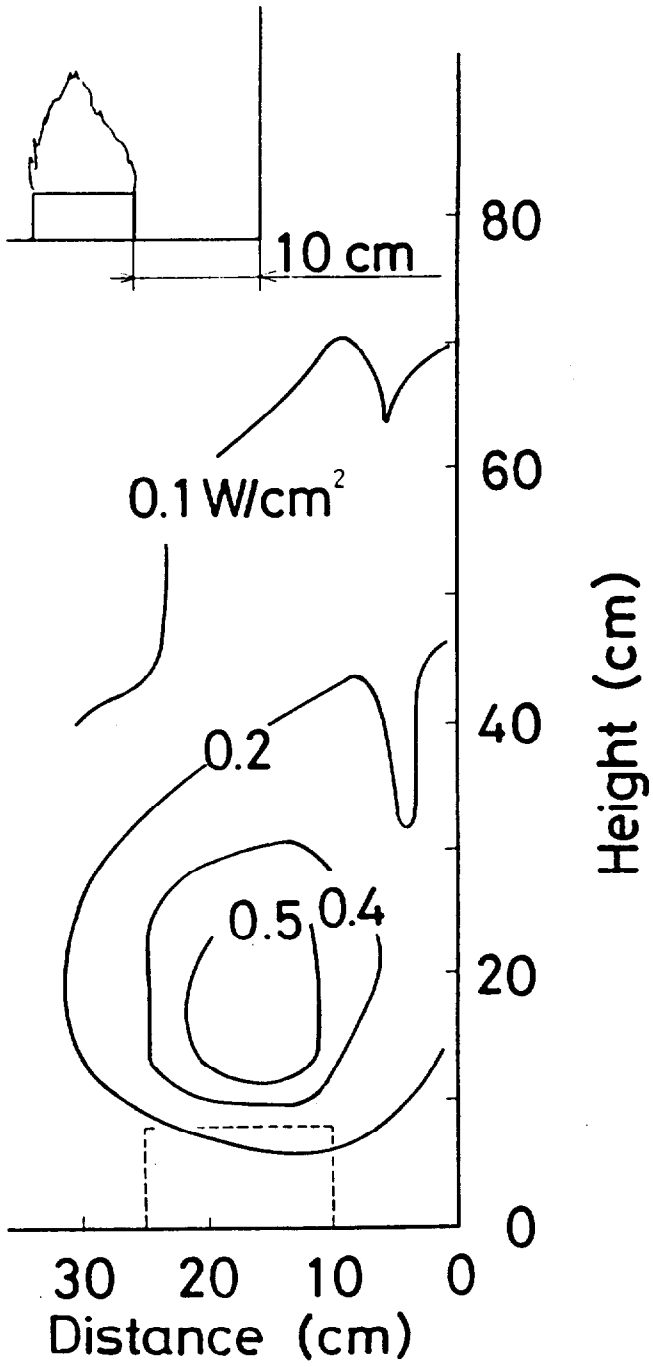
10 cm
80
0.1 W/cm²
60
0.2
40
0.5
0.4
20
0
30
20
10
0
Distance (cm)
Height (cm)

Fig. 6c

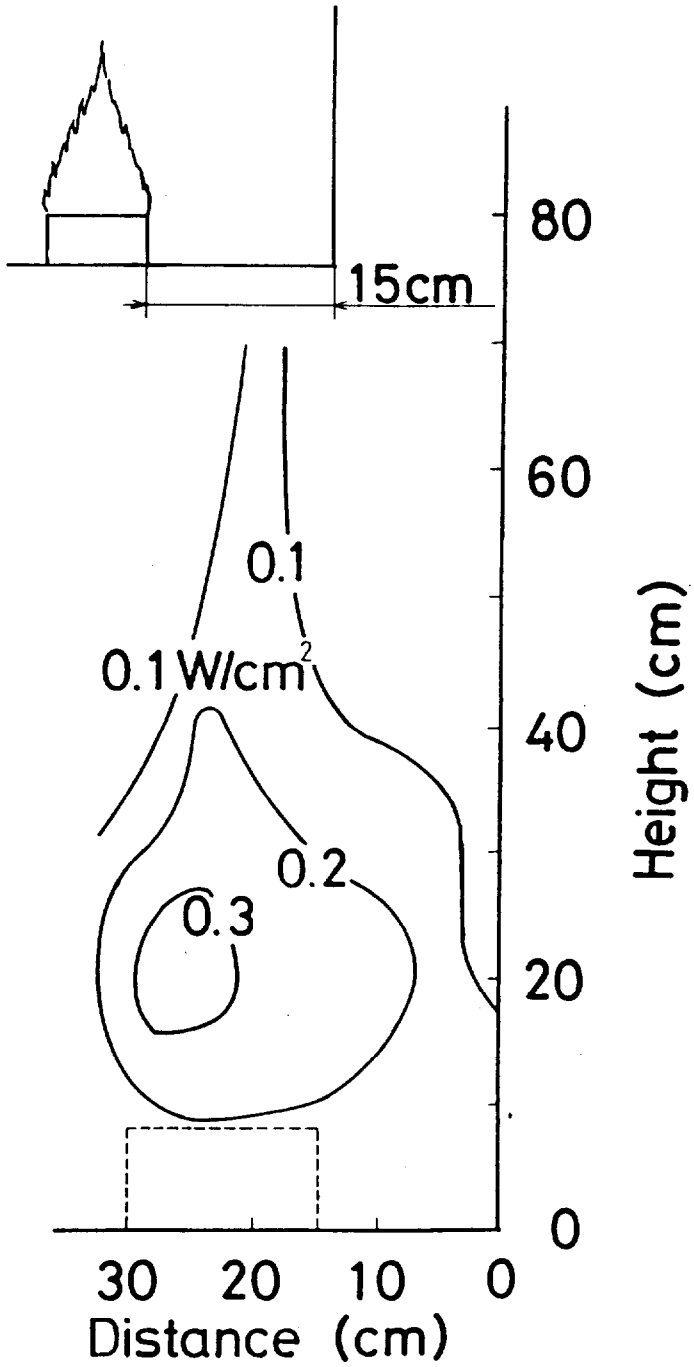
15cm
80
60
40
20
0
0.1
0.1W/cm²
0.2
0.3
Height (cm)
30 20 10 0
Distance (cm)

Fig. 6d

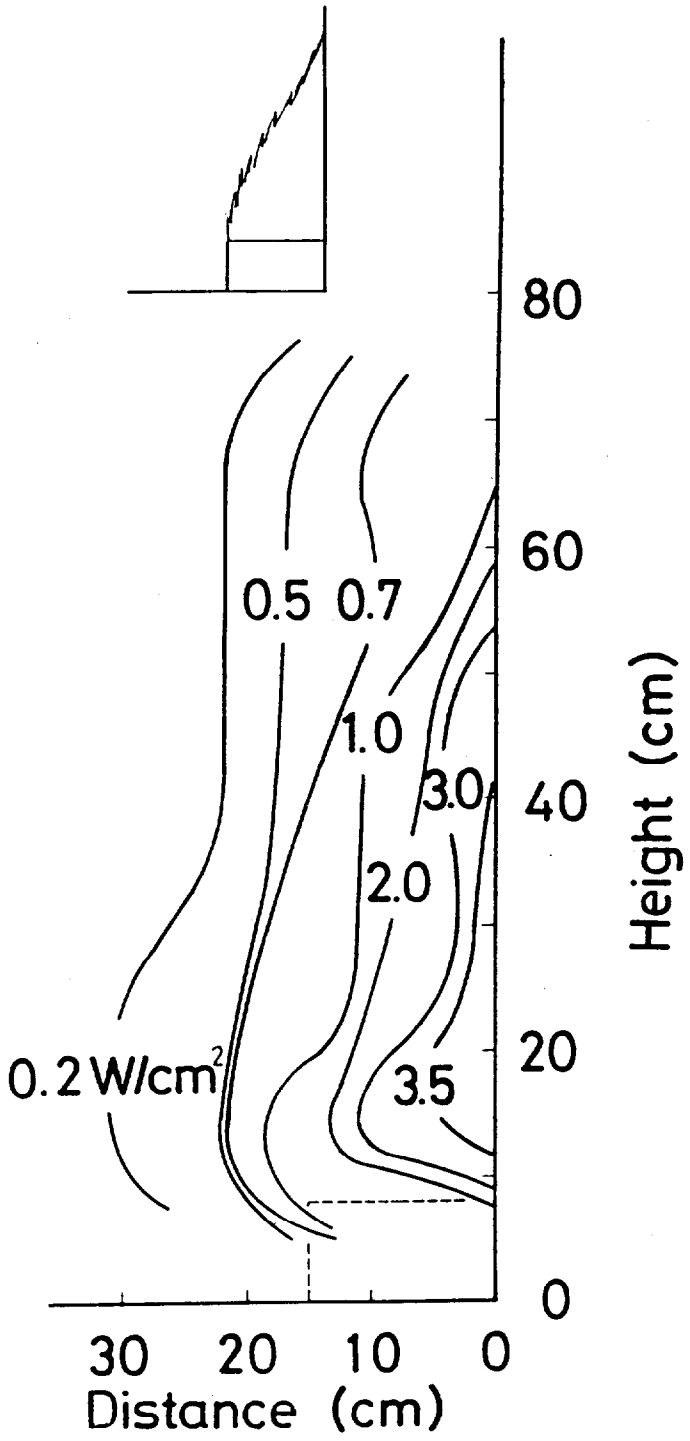
80
60
40
20
0
Height (cm)
0.5
0.7
1.0
3.0
2.0
3.5
0.2 W/cm²
30
20
10
0
Distance (cm)

Fig. 7a

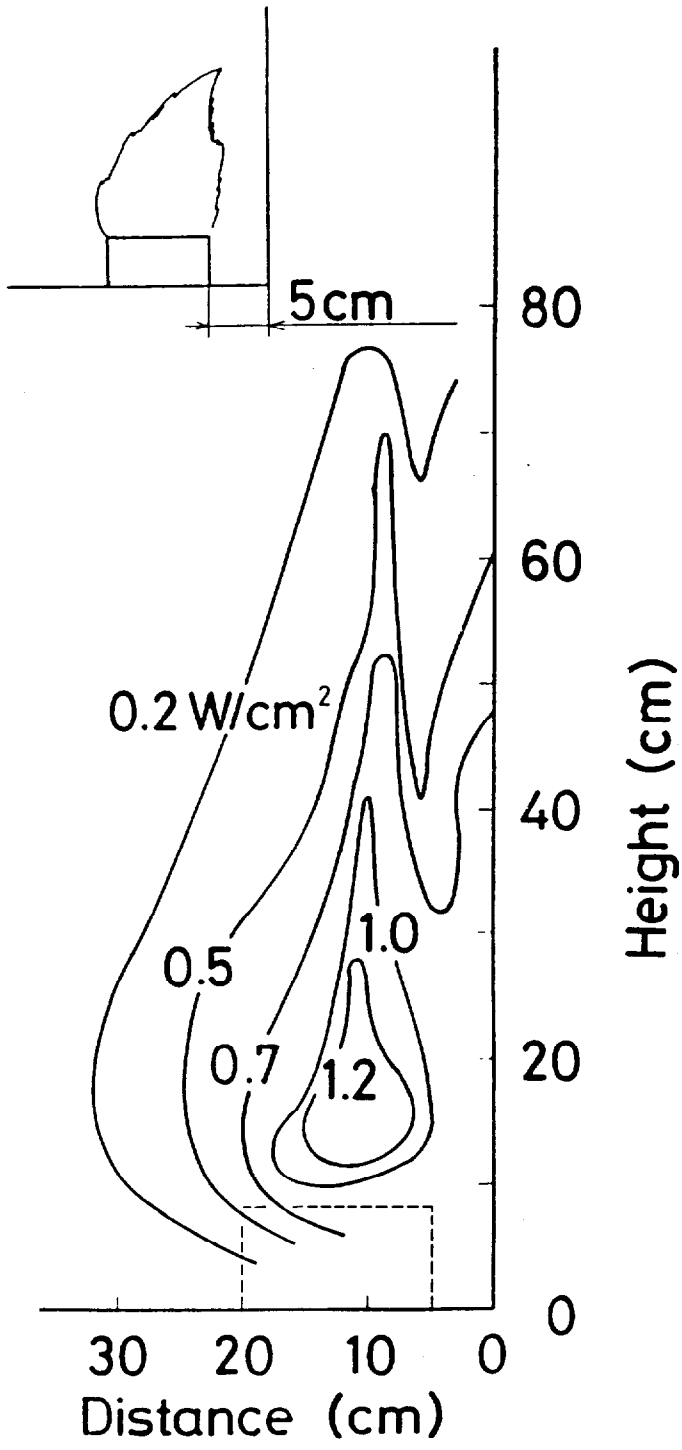
5cm
80
60
40
20
0
0.2 W/cm²
0.5
0.7
1.0
1.2
Height (cm)
30
20
10
0
Distance (cm)

Fig. 7b

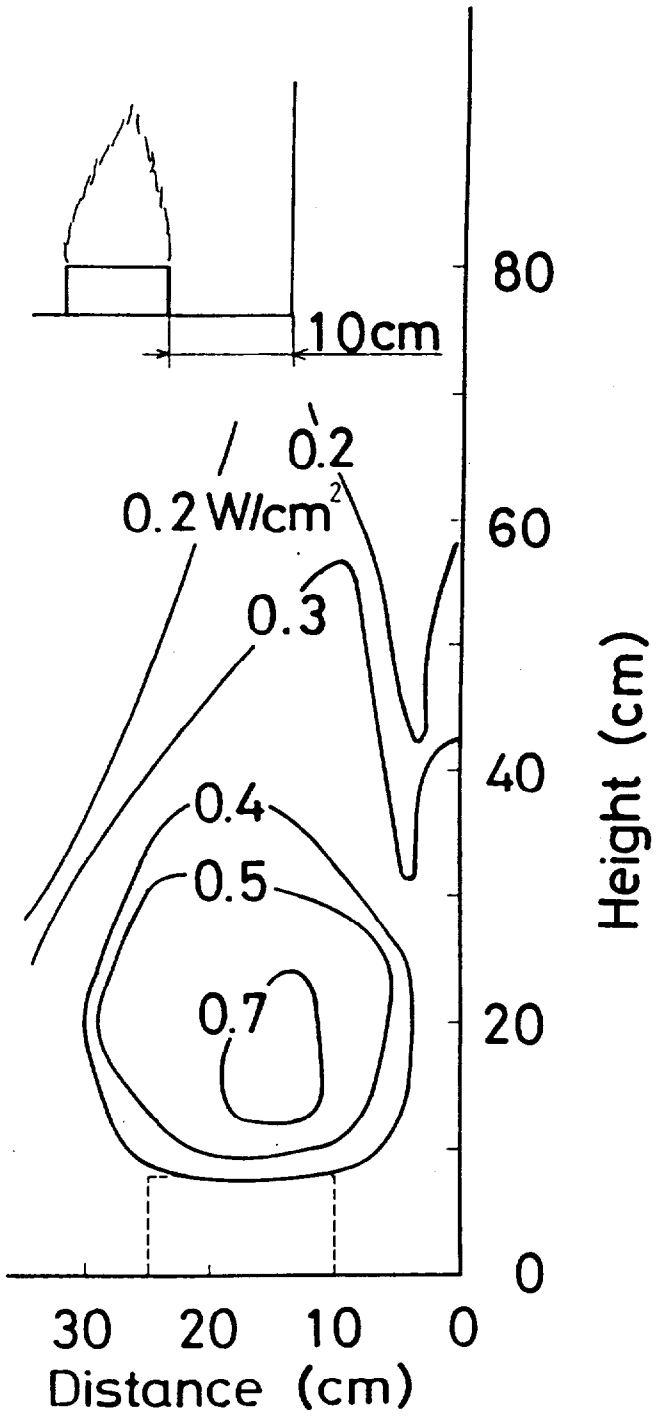
10cm
0.2
0.2 W/cm²
0.3
0.4
0.5
0.7
80
60
40
20
0
Height (cm)
30
20
10
0
Distance (cm)

Fig. 7c

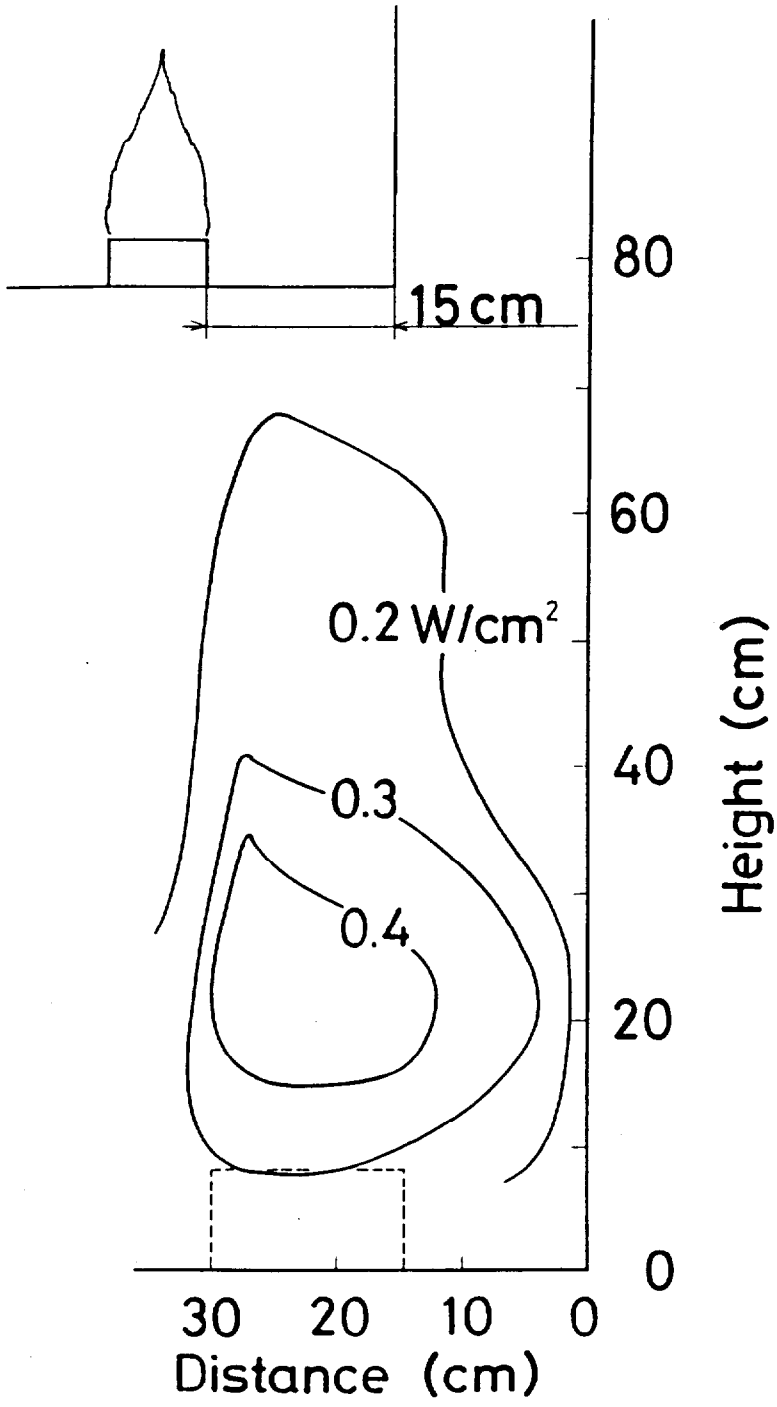

Fig. 7d

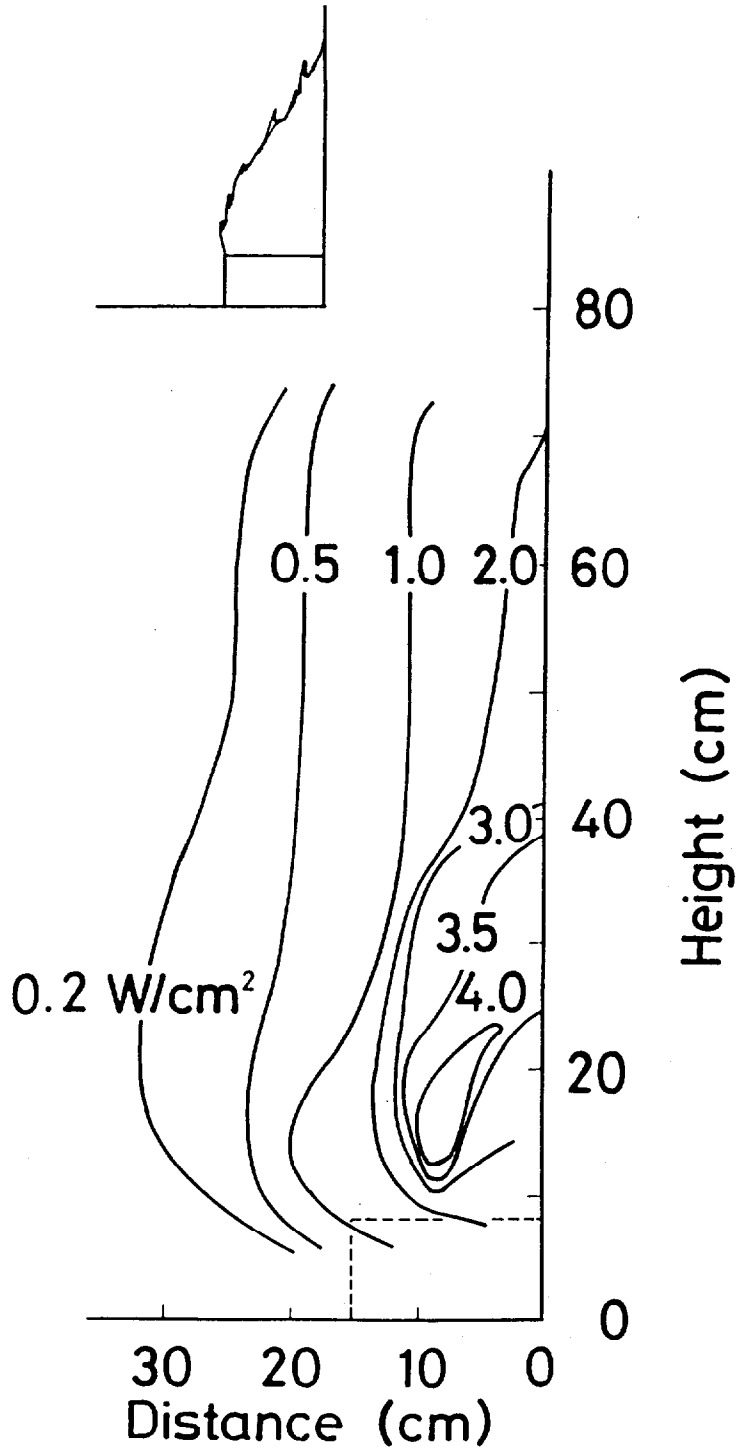
80
60
40
20
0
Height (cm)
0.5
1.0
2.0
3.0
3.5
4.0
0.2 W/cm²
30
20
10
0
Distance (cm)

Fig. 8a

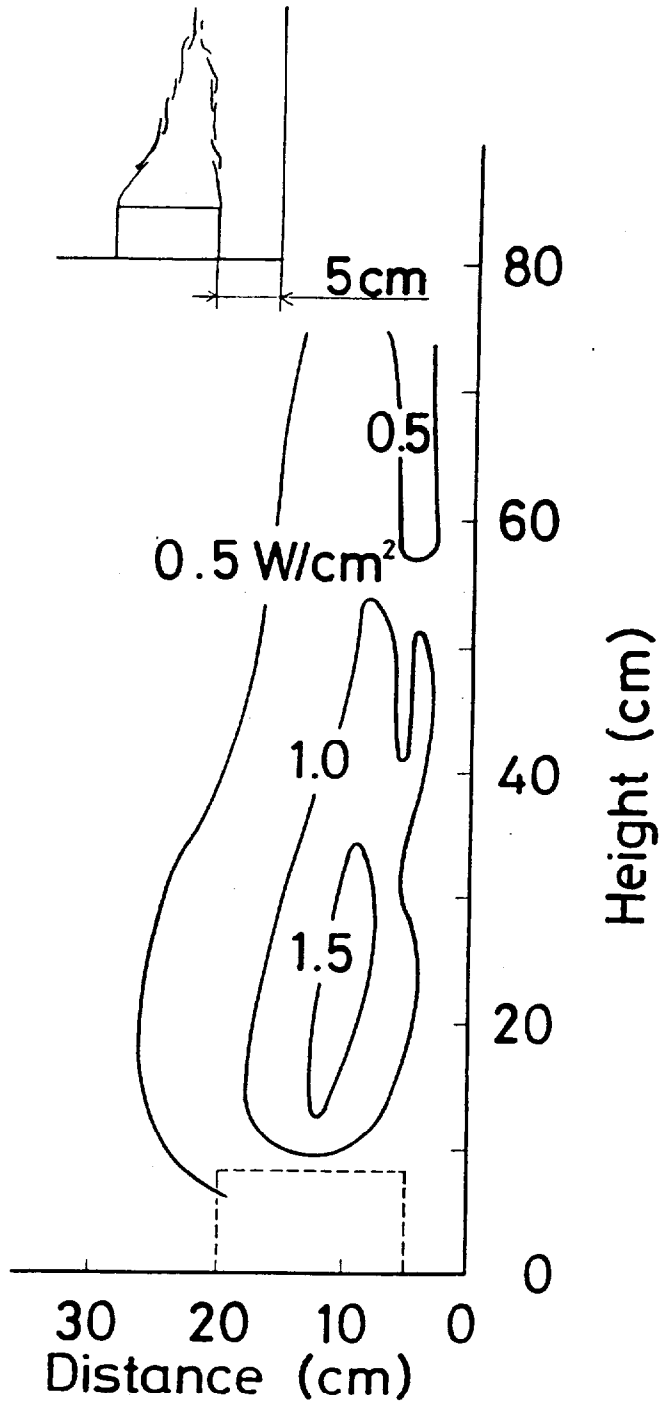

Fig. 8b

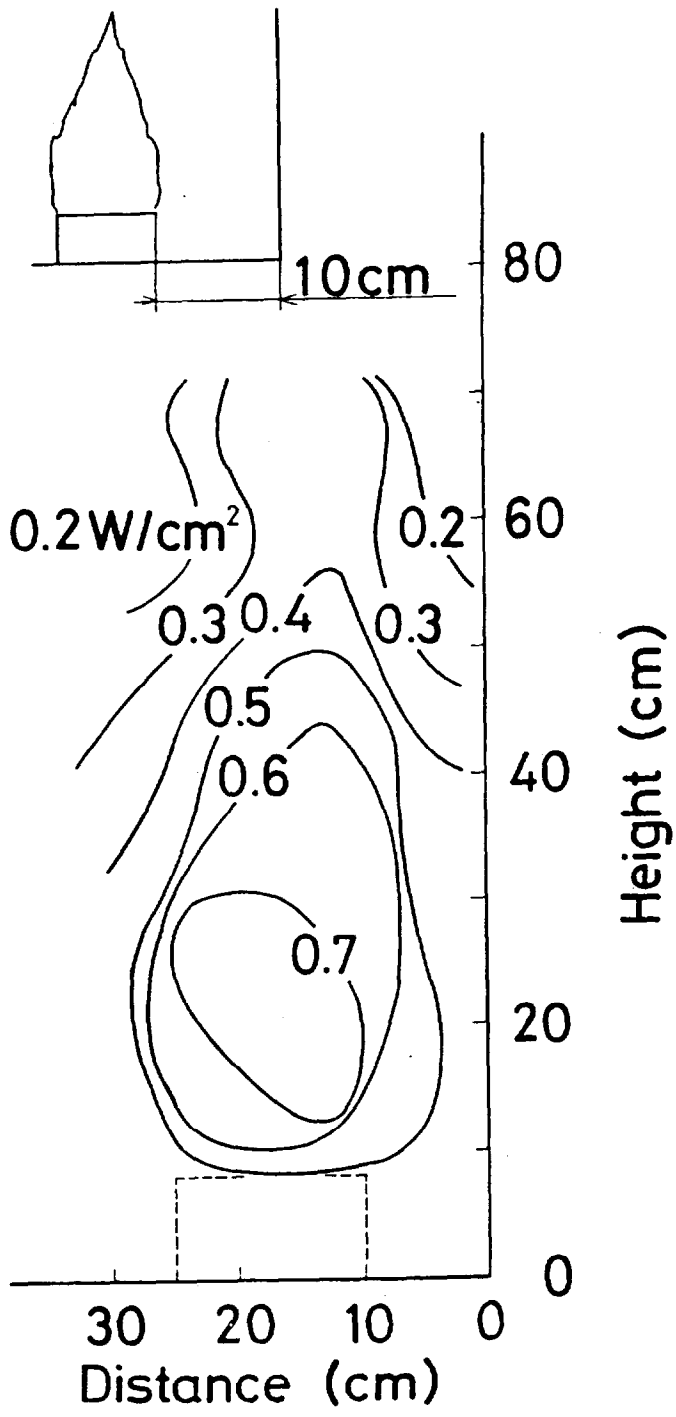
10cm
80
0.2W/cm²
0.2
60
0.3
0.4
0.3
0.5
0.6
40
0.7
20
0
30
20
10
0
Distance (cm)
Height (cm)

Fig. 8c

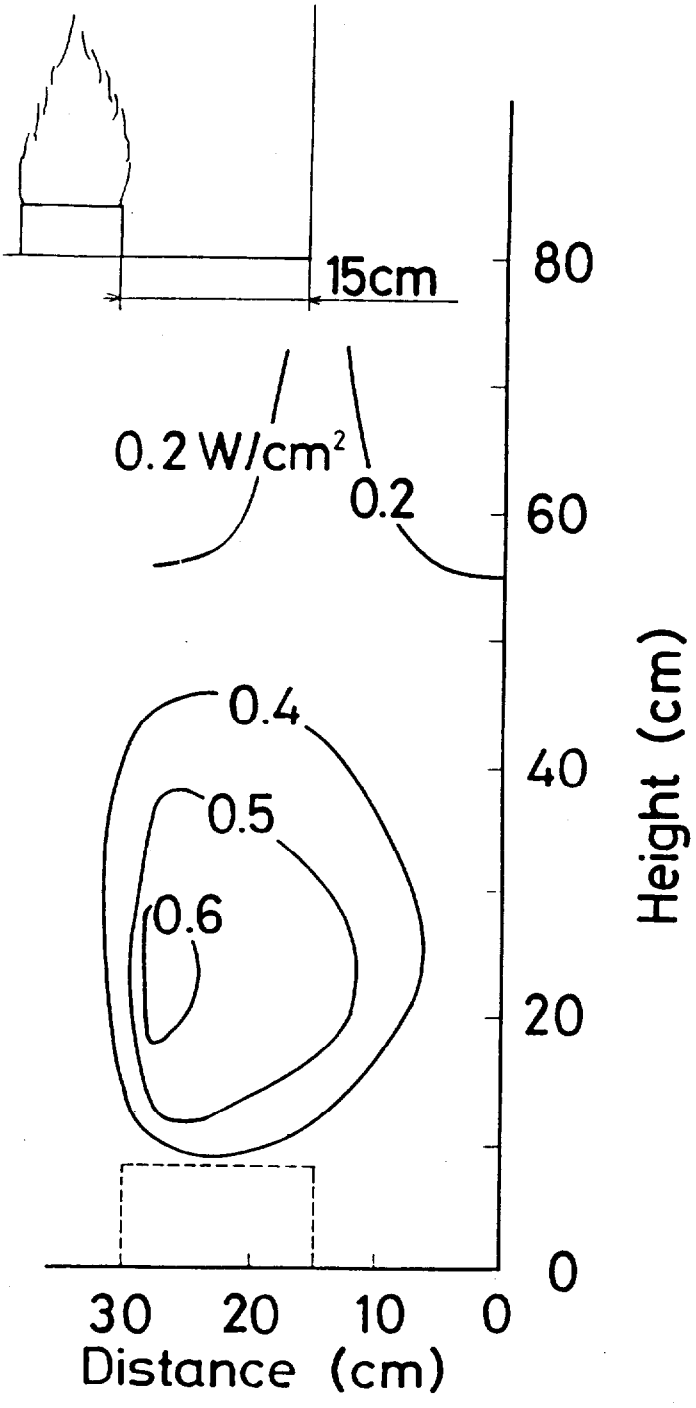
15cm
0.2 W/cm²
0.2
0.4
0.5
0.6
80
60
40
20
0
Height (cm)
30
20
10
0
Distance (cm)

Fig. 8d

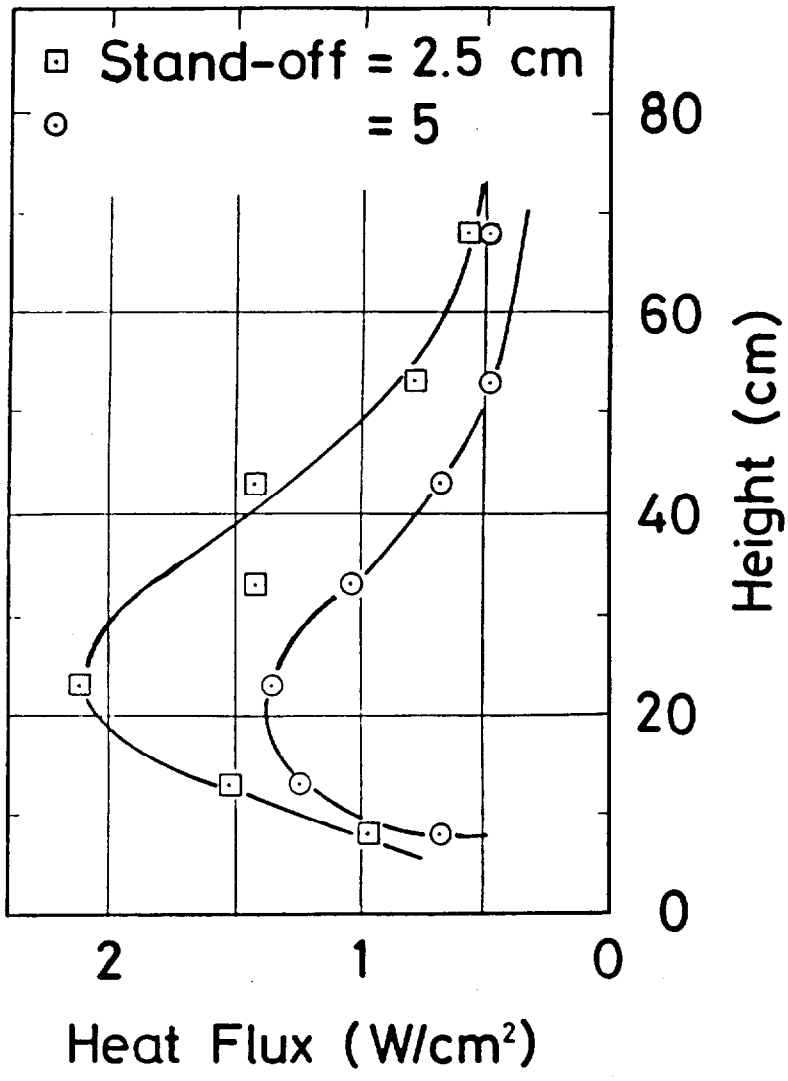

Fig. 9

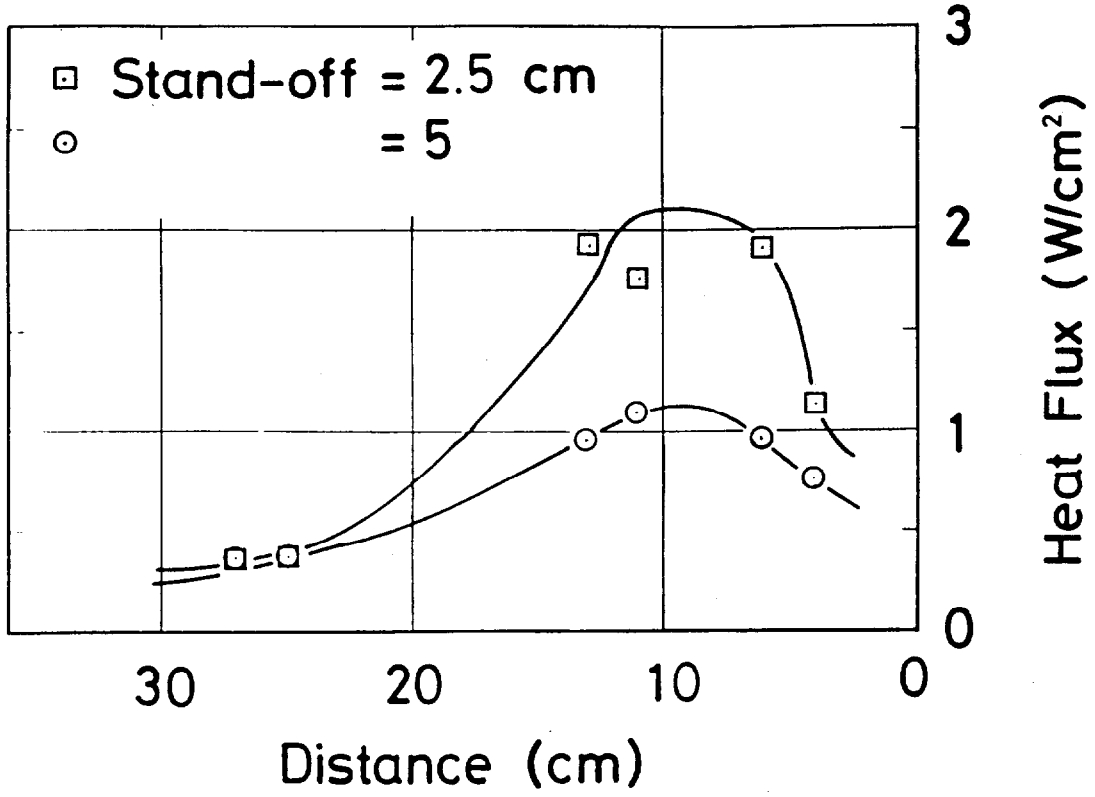

Fig. 10

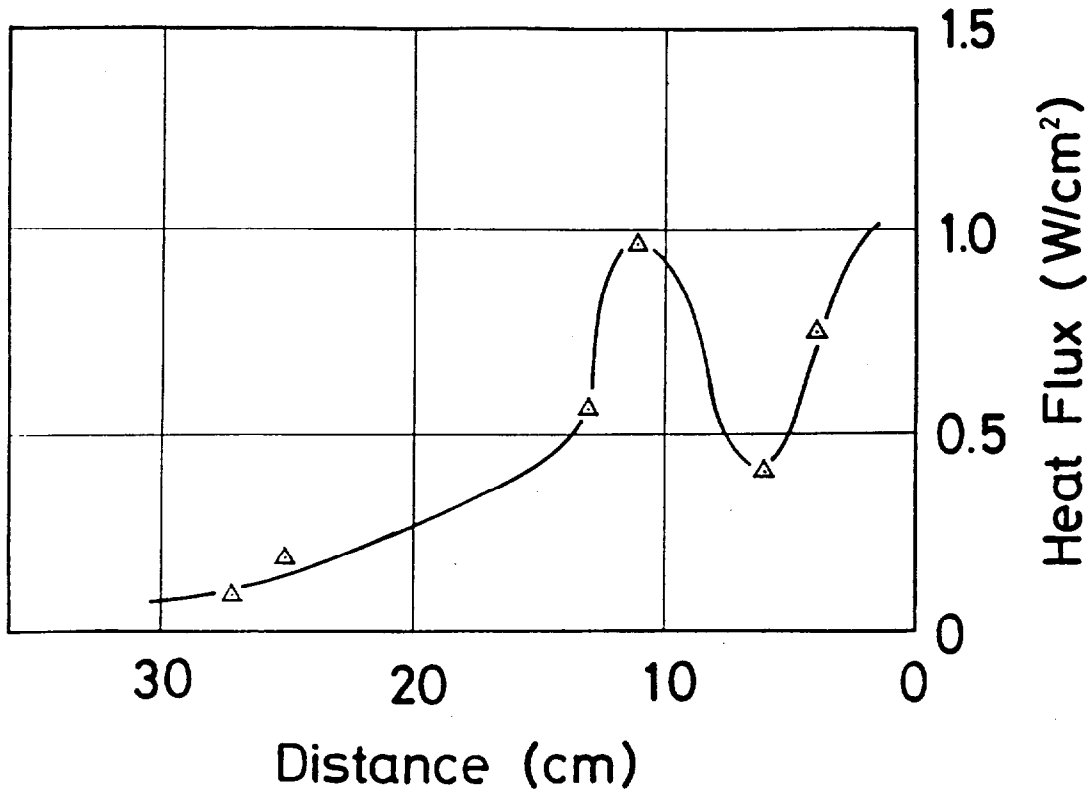

Fig. 11

APPENDIX – B

Flame Height Measurement

The history of visible flame shape was recorded in a video camera system using the same room corner model as used for the measurements in Appendix A. Visible flame height was then obtained by averaging the flame tip height. The frequency of flame fluctuation was estimated from the video film to be approximately a few Hz, therefore, three second averaging time period was used to obtain the average flame height. The flame height measurements were performed changing the burner heat release rate between 4.5 and 31.5 kW and the burner stand–off distance between 0 and 25 cm. Figure 12 shows average flame height as a function of burner heat release rate for three different burner stand–off distances. Figure 13 shows the average flame height as a function of burner stand–off distance for two different burner heat release rates.

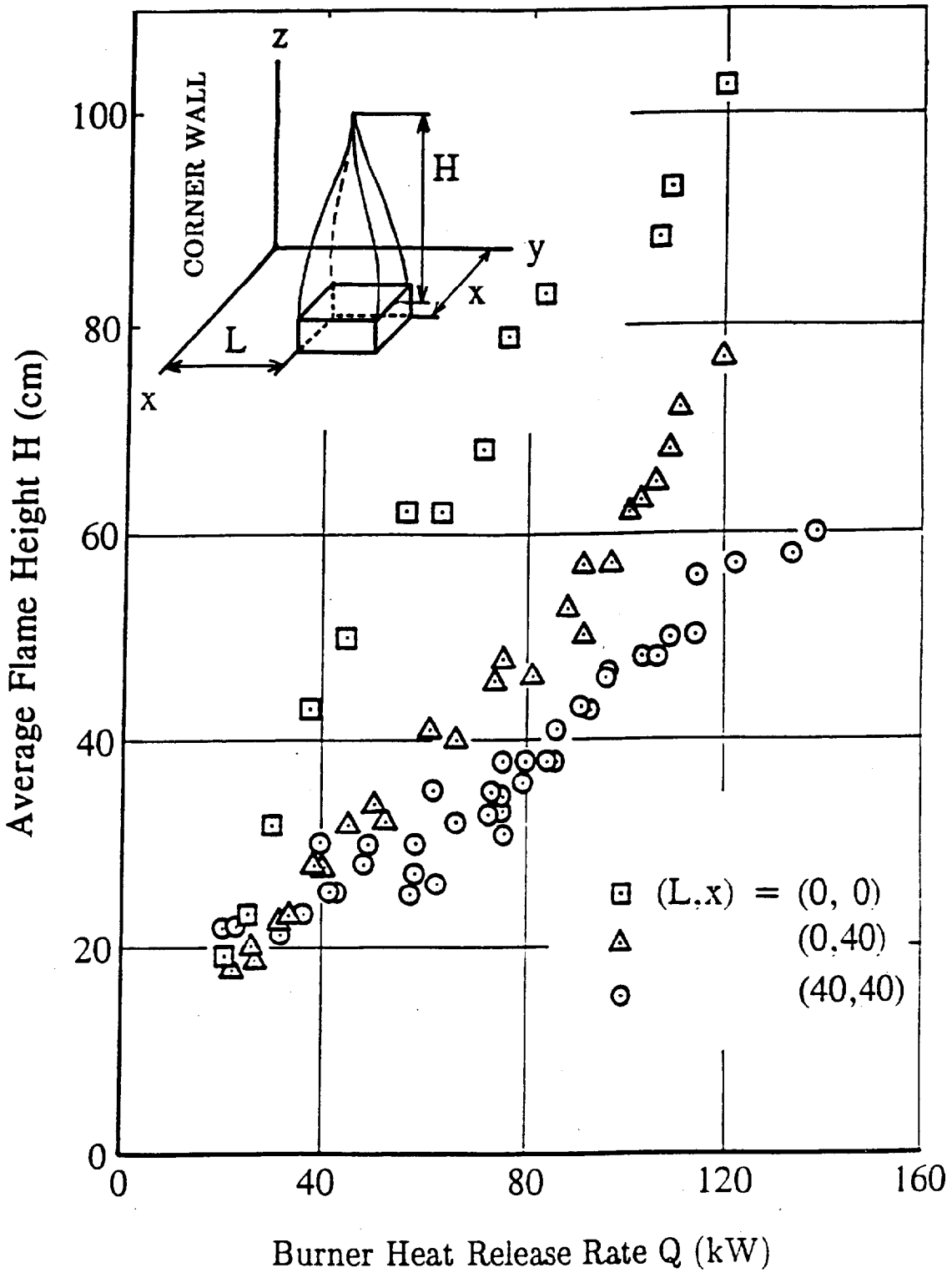
Average Flame Height H (cm)
Burner Heat Release Rate Q (kW)
0
20
40
60
80
100
0
40
80
120
160
CORNER WALL
z
H
y
x
L
x
(L,x) = (0, 0)
(0,40)
(40,40)

Fig. 12

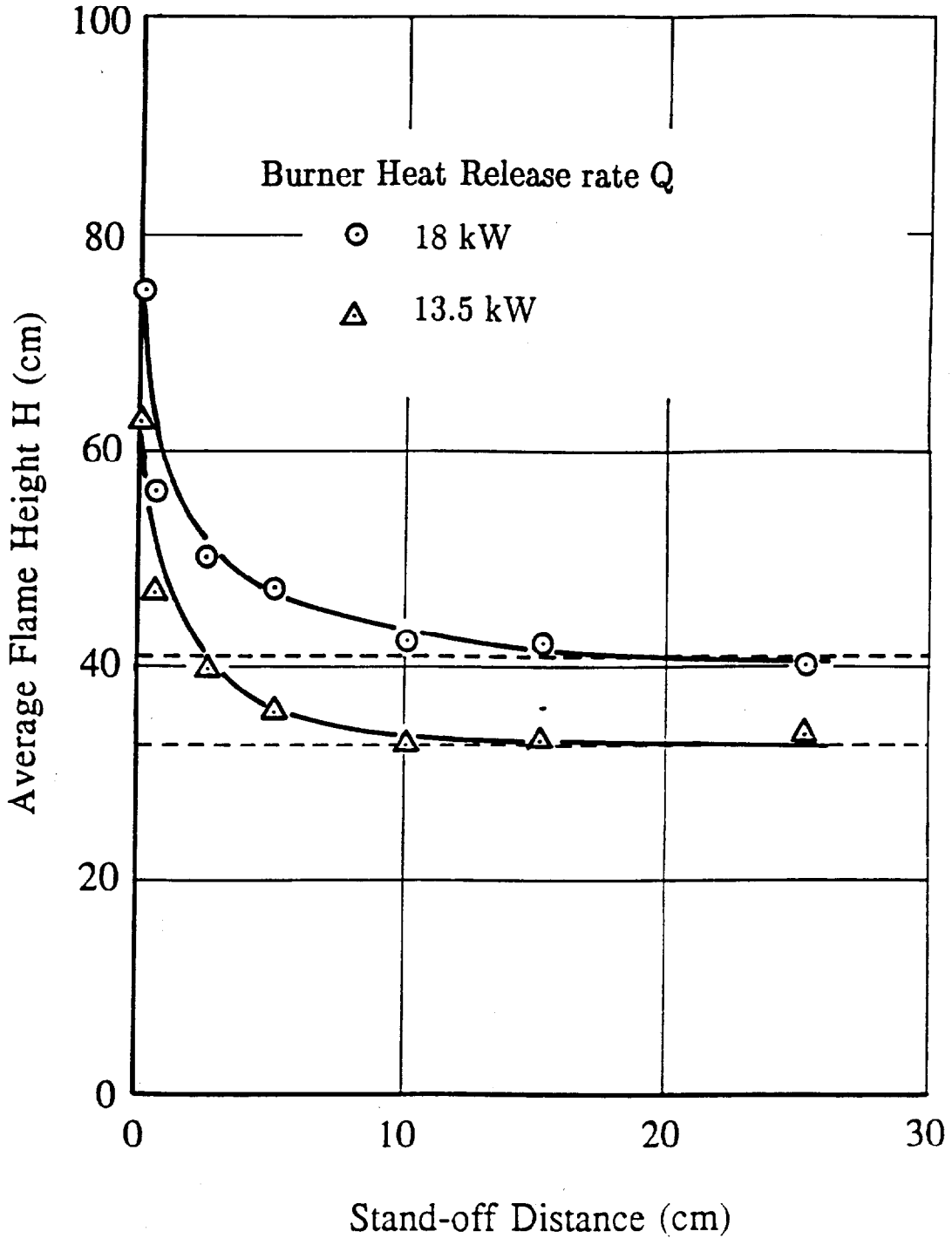
100
80
60
40
20
0
Average Flame Height H (cm)
Burner Heat Release rate Q
18 kW
13.5 kW
0
10
20
30
Stand-off Distance (cm)

Fig. 13

NIST-114
(REV. 9-92)
ADMAN 4.09

U.S. DEPARTMENT OF COMMERCE
NATIONAL INSTITUTE OF STANDARDS AND TECHNOLOGY

MANUSCRIPT REVIEW AND APPROVAL

(ERB USE ONLY)
ERB CONTROL NUMBER | DIVISION
PUBLICATION REPORT NUMBER: NIST-GCR-93-628 | CATEGORY CODE
PUBLICATION DATE: April 1993 | NUMBER PRINTED PAGES

INSTRUCTIONS: ATTACH ORIGINAL OF THIS FORM TO ONE (1) COPY OF MANUSCRIPT AND SEND TO: THE SECRETARY, APPROPRIATE EDITORIAL REVIEW BOARD.

TITLE AND SUBTITLE (CITE IN FULL)

Study of Fire Induced Flow Along the Vertical Corner Wall. Part 2

CONTRACT OR GRANT NUMBER
60NANB1D1142

TYPE OF REPORT AND/OR PERIOD COVERED
Final Report

AUTHOR(S) (LAST NAME, FIRST INITIAL, SECOND INITIAL)

Kozo Saito
University of Kentucky
Department of Mechanical Engineering
Lexington, KY 40506-0108

PERFORMING ORGANIZATION (CHECK (X) ONE BOX)
[ ] NIST/GAITHERSBURG
[ ] NIST/BOULDER
[ ] JILA/BOULDER

LABORATORY AND DIVISION NAMES (FIRST NIST AUTHOR ONLY)

SPONSORING ORGANIZATION NAME AND COMPLETE ADDRESS (STREET, CITY, STATE, ZIP)

U.S. Department of Commerce
National Institute of Standards and Technology
Gaithersburg, MD 20899

RECOMMENDED FOR NIST PUBLICATION
[ ] JOURNAL OF RESEARCH (NIST JRES)
[ ] J. PHYS. & CHEM. REF. DATA (JPCRD)
[ ] HANDBOOK (NIST HB)
[ ] SPECIAL PUBLICATION (NIST SP)
[ ] TECHNICAL NOTE (NIST TN)
[ ] MONOGRAPH (NIST MN)
[ ] NATL. STD. REF. DATA SERIES (NIST NSRDS)
[ ] FEDERAL INF. PROCESS. STDS. (NIST FIPS)
[ ] LIST OF PUBLICATIONS (NIST LP)
[ ] NIST INTERAGENCY/INTERNAL REPORT (NISTIR)
[ ] LETTER CIRCULAR
[ ] BUILDING SCIENCE SERIES
[ ] PRODUCT STANDARDS
[X] OTHER NIST-GCR-

RECOMMENDED FOR NON-NIST PUBLICATION (CITE FULLY) [ ] U.S. [ ] FOREIGN

PUBLISHING MEDIUM
[X] PAPER [ ] CD-ROI
[ ] DISKETTE (SPECIFY)
[ ] OTHER (SPECIFY)

SUPPLEMENTARY NOTES

ABSTRACT (A 1500-CHARACTER OR LESS FACTUAL SUMMARY OF MOST SIGNIFICANT INFORMATION. IF DOCUMENT INCLUDES A SIGNIFICANT BIBLIOGRAPHY OR LITERATURE SURVEY, CITE IT HERE. SPELL OUT ACRONYMS ON FIRST REFERENCE.) (CONTINUE ON SEPARATE PAGE, IF NECESSARY.)

This paper describes a new experimental technique with wide application which has been proven for corner fires. To measure the flame spread rate of pyrolysis front along vertically oriented flat and corner walls, it may be necessary to measure transient temperature profiles on the walls. Conventional thermocouple and visual observation methods, however, have limitation due to complexity of implementation and the inherent ambiguity of visual observations due to interference from flames. To overcome these limitations, automated infrared imaging was applied for simultaneously collecting temperature data in a relatively large wall surface area. Results indicate that the infrared system with a (10.6 $\pm$ 0.5μm) band-pass filter successfully avoids the flame interference allowing measurements of temperature distribution on the fire-heated wall, from which the spread rate in any direction can be deduced. The infrared camera without filters also can be used to measure visible flame position as photographic and video camera.

KEY WORDS (MAXIMUM 9 KEY WORDS; 28 CHARACTERS AND SPACES EACH; ALPHABETICAL ORDER; CAPITALIZE ONLY PROPER NAMES)

building fires; corner tests; flame height; flame spread rate; heat flux; infrared photography; room fires; walls

AVAILABILITY
[X] UNLIMITED [ ] FOR OFFICIAL DISTRIBUTION. DO NOT RELEASE TO NTIS.
[ ] ORDER FROM SUPERINTENDENT OF DOCUMENTS, U.S. GPO, WASHINGTON, D.C. 20402
[X] ORDER FROM NTIS, SPRINGFIELD, VA 22161

NOTE TO AUTHOR(S) IF YOU DO NOT WISH THIS MANUSCRIPT ANNOUNCED BEFORE PUBLICATION, PLEASE CHECK HERE. [ ]

ELECTRONIC FORM